



# Thermal properties, geometrical structures, antimicrobial activity and DNA binding of supramolecular azo dye complexes



A.Z. El-Sonbati\*, M.A. Diab, A.A. El-Bindary, A.F. Shoair, N.M. Beshry

Chemistry Department, Faculty of Science, Damietta University, Damietta, Egypt

## ARTICLE INFO

### Article history:

Received 1 January 2016

Accepted 20 February 2016

Available online xxxx

### Keywords:

Molecular structures

Molecular docking

Antimicrobial activity

Catalytic oxidation

Thermodynamic parameters

## ABSTRACT

Ru(III) complexes of 5-(4-derivative phenyl azo)-8-hydroxyquinoline (HL<sub>n</sub>) are prepared and characterized by elemental analyses, IR, UV–Visible spectra, <sup>1</sup>H and <sup>13</sup>C NMR spectra, mass spectra, X-ray diffraction analysis, conductivity measurements and magnetic susceptibility measurements as well as thermal analysis. The XRD patterns show that the ligand (HL<sub>3</sub>) has a polycrystalline nature and complex (2) is completely amorphous. The ligands act as a monobasic bidentate coordinating through CN and OH groups by replacement of a proton from the latter group. The molar conductivities show that the Ru(III) complexes are non-electrolyte in nature. The spectra show that all complexes are octahedral in which two chlorides are attached to the metal ion. The optimized bond lengths, bond angles and the calculated quantum chemical parameters for the ligands (HL<sub>n</sub>) and Ru(III) complexes are investigated. Molecular docking was used to predict the binding between azo dye ligands and the receptor of prostate cancer mutant 2q7k-hormone. The activation thermodynamic parameters, such as activation energy (E<sub>a</sub>), enthalpy (ΔH<sup>‡</sup>), entropy (ΔS<sup>‡</sup>) and Gibbs free energy change of the decomposition (ΔG<sup>‡</sup>) are calculated using Coats–Redfern and Horowitz–Metzger methods. The ligands (HL<sub>n</sub>) and Ru(III) complexes are screened for their antimicrobial activity against bacterial and fungal species. The tested complexes (1) and (2) have good antibacterial activity against *Bacillus cereus* and the tested ligands (HL<sub>2</sub>, HL<sub>3</sub> and HL<sub>5</sub>) have good antifungal activity against *Aspergillus niger* and also HL<sub>5</sub> showed against *Alternaria alternata*. The catalytic oxidation of cyclohexanol by [Ru(L<sub>n</sub>)(AsPh<sub>3</sub>)<sub>2</sub>Cl<sub>2</sub>]·xH<sub>2</sub>O with periodic acid as co-oxidant is described. The Ru(III) complexes exhibited a catalytic activity for the oxidation of cyclohexanol to cyclohexanon.

© 2016 Elsevier B.V. All rights reserved.

## 1. Introduction

Considerable interest has been focused on the synthesis of the azo dye compounds and its metal complex due to its wide potential applications. The chemistry of azo quinoline and its derivatives has attracted special interest due to their environmental stability and their promising optical and electrical properties [1–4]. Our interest in the supramolecular chemistry of 8-hydroxyquinoline derivatives arises from their versatility [5] as well as the hydrogen bonding ability of these molecules [6,7].

The azo compounds continue to occupy an important position as ligands in metal coordination chemistry even after almost a century since their discovery. Nitrogen and oxygen atoms have long been used to increase the biological activity of organic moiety [8] and quinoline compounds have also found applications in medicinal chemistry [9]. The number and diversity of nitrogen and oxygen chelating agents used to prepare new coordination and organometallic compounds have increased rapidly recently [10].

8-Hydroxyquinoline derivatives and their complexes with transition metals have high antibacterial activities [11,12]. Also, the chemical properties of quinoline have been widely discussed because of their biological relevance [12]. They have attracted special interest due to their therapeutic properties. Quinoline azo dye and its derivatives are very important compounds and have attracted much attention in both academic and applied research used in many applications such as chromophoric and metallochromic indicators in analytical chemistry [13].

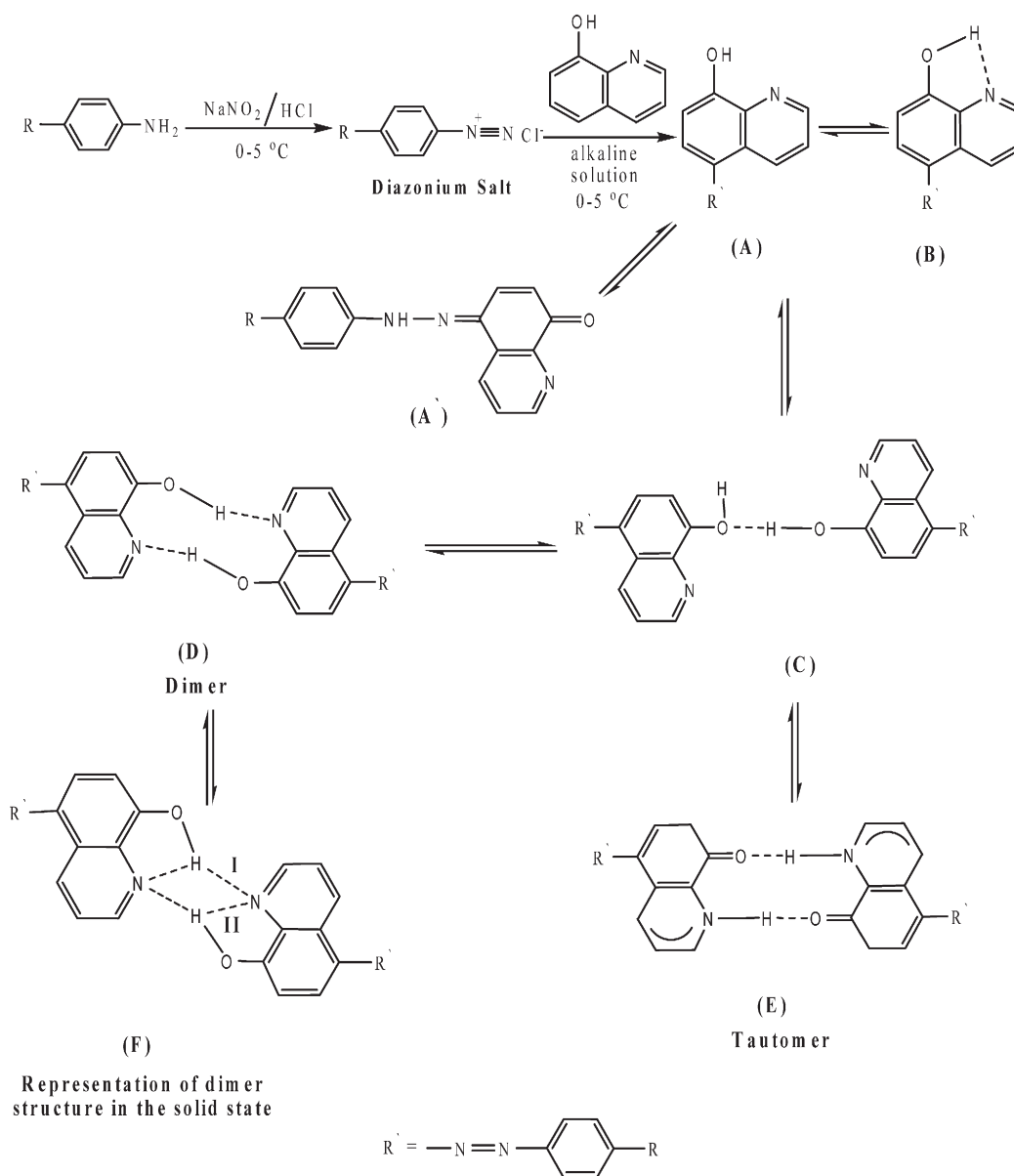
Also, azo compounds based on quinoline play a central role as chelating agents for a large number of metal ions, as they form a stable six and/or five-membered ring after complexation with the metal ion [1–4,14,15].

Ruthenium complexes have gained interest and impressive development in last decades for many reasons, especially due to their catalytic properties [16]. Ruthenium generally demonstrates affinity toward N-donor molecules such as proteins and DNA. Ruthenium (III) complexes with numerous different ligands are reasonably synthesized and investigated for the purpose of possible application in medicine and catalysis.

This paper describes the characterization of 5-(4-derivative phenyl azo)-8-hydroxyquinoline ligands and Ru(III) complexes by elemental

\* Corresponding author.

E-mail address: [elsonbaticsh@yahoo.com](mailto:elsonbaticsh@yahoo.com) (A.Z. El-Sonbati).



$n=1$ ,  $R = OCH_3$  (HL<sub>1</sub>);  $n=2$ ,  $CH_3$  (HL<sub>2</sub>);  $n=3$ ,  $H$  (HL<sub>3</sub>);  $n=4$ ,  $Cl$  (HL<sub>4</sub>); and  $n=5$ ,  $NO_2$  (HL<sub>5</sub>)

**Scheme 1.** The formation mechanism of quinoline azo dye derivatives (HL<sub>n</sub>) [intramolecular (B, F) and intermolecular hydrogen bonding (C–F)].

analyses, IR, <sup>1</sup>H NMR, <sup>13</sup>C NMR, UV–Vis spectra, X-ray diffraction, magnetic moment, molar conductance, and thermal analyses. Molecular and electronic structures of the ligands (HL<sub>n</sub>) are discussed. Mass spectra and X-ray diffraction analysis of ligand (HL<sub>3</sub>) are discussed. We studied the antimicrobial activity of the ligands (HL<sub>n</sub>) and Ru(III) complexes and compared antimicrobial activity results of ligands and

Ru(III) complexes with the standard antibacterial and antifungal drugs. The activation thermodynamic parameters were calculated using Coats–Redfern and Horowitz–Metzger methods. The calf thymus DNA binding activity of the ligands (HL<sub>n</sub>) and Ru(III) complexes was studied by absorption spectra as well as the catalytic oxidation of cyclohexanol by [Ru(L<sub>n</sub>)(AsPh<sub>3</sub>)<sub>2</sub>Cl<sub>2</sub>]·xH<sub>2</sub>O with periodic acid as co-oxidant.

**Table 1**  
Analytical and physical data of the ligands (HL<sub>n</sub>) and Ru(III) complexes (1–3).

Compound	Empirical formula	Yield (%)	m.p. (°C)	Exp. (calc.) %			
				C	H	N	M
HL <sub>1</sub>	C <sub>16</sub> H <sub>13</sub> N <sub>3</sub> O <sub>2</sub>	65	152	68.64 (68.82)	4.52 (4.66)	14.84 (15.05)	–
HL <sub>2</sub>	C <sub>16</sub> H <sub>13</sub> N <sub>3</sub> O	68	172	72.87 (73.00)	4.78 (4.94)	15.67 (15.97)	–
HL <sub>3</sub>	C <sub>15</sub> H <sub>11</sub> N <sub>3</sub> O	71	188	72.12 (72.29)	4.20 (4.42)	16.51 (16.87)	–
HL <sub>4</sub>	C <sub>15</sub> H <sub>10</sub> N <sub>3</sub> OCl	77	215	63.26 (63.49)	3.32 (3.53)	14.44 (14.82)	–
HL <sub>5</sub>	C <sub>15</sub> H <sub>10</sub> N <sub>4</sub> O <sub>3</sub>	81	274	61.11 (61.23)	3.32 (3.40)	18.85 (19.05)	–
(1)	[Ru(L <sub>1</sub> )(As(Ph) <sub>3</sub> ) <sub>2</sub> Cl <sub>2</sub> ]·2H <sub>2</sub> O	44	138	56.56 (56.83)	3.65 (3.83)	3.54 (3.83)	8.88 (9.20)
(2)	[Ru(L <sub>3</sub> )(As(Ph) <sub>3</sub> ) <sub>2</sub> Cl <sub>2</sub> ]·2H <sub>2</sub> O	52	142	57.13 (57.30)	3.55 (3.75)	3.76 (3.93)	9.17 (9.46)
(3)	[Ru(L <sub>5</sub> )(As(Ph) <sub>3</sub> ) <sub>2</sub> Cl <sub>2</sub> ]	45	140	56.64 (56.82)	3.46 (3.62)	4.87 (5.20)	9.13 (9.38)

## 2. Experimental techniques

### 2.1. Synthesis of quinoline azo dye ligands

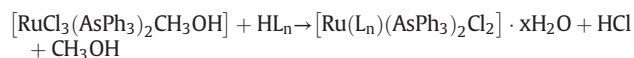
5-(4-Derivative phenyl azo)-8-hydroxyquinoline ligands (HL<sub>n</sub>) are prepared according to El-Sonbati et al. [17,18]. In a typical preparation, 25 ml of distilled water containing 0.01 mol hydrochloric acid are added to aniline (0.01 mol) or *p*-derivatives. A solution of 0.01 mol sodium nitrite in 20 ml of water is added dropwise to the resulting mixture then stirred and cooled to 0 °C. The formed diazonium chloride is consecutively coupled with an alkaline solution of 0.01 mol quinoline-8-ol, in 10 ml of pyridine. The preparation of ligands (HL<sub>n</sub>) is summarized in Scheme 1. The colored precipitate, which formed immediately, is filtered through sintered glass crucible and washed several times with water. The crude products are purified by recrystallization from hot ethanol and dried in vacuum desiccator over P<sub>2</sub>O<sub>5</sub>. The ligands are also characterized by IR, <sup>1</sup>H and <sup>13</sup>C NMR spectroscopy and elemental analysis (Table 1). Yield percent was 65–81%.

The resulting formed ligands are:

HL <sub>1</sub>	5-(4-methoxyphenyl azo)-8-hydroxyquinoline.
HL <sub>2</sub>	5-(4-methylphenyl azo)-8-hydroxyquinoline.
HL <sub>3</sub>	5-(phenyl azo)-8-hydroxyquinoline.
HL <sub>4</sub>	5-(4-chlorophenyl azo)-8-hydroxyquinoline.
HL <sub>5</sub>	5-(4-nitrophenyl azo)-8-hydroxyquinoline.

### 2.2. Preparation of Ru(III) complexes

All Ru(III) complexes are prepared according to the general procedure [19]. A stoichiometric amount of the desired ligand (0.01 mol) in DMF is added dropwise to a solution of [RuCl<sub>3</sub>(AsPh<sub>3</sub>)<sub>2</sub>CH<sub>3</sub>OH] (0.01 mol) in DMF with stirring and the reaction mixture is refluxed for 4 h. The solution is concentrated to half of its original volume by evaporation and allowed to cool at room temperature. Micro crystalline precipitates are separated and dried in a vacuum desiccator over anhydrous CaCl<sub>2</sub>. The structure of the prepared complexes is present in Fig. 1. The complexes are characterized by IR spectroscopy and elemental analyses (Table 1). Yield percent was 44–52%.



where  $n = 1, 3; x = 2$  and  $n = 5; x = 0$

### 2.3. DNA binding experiments

The binding properties of the ligands and their complexes to CT-DNA are studied using electronic absorption spectroscopy. The stock solution of CT-DNA is prepared in 5 mM Tris-HCl/50 mM NaCl buffer (pH = 7.2), with a ratio of UV absorbances at 260 and 280 nm ( $A_{260}/A_{280}$ ) of ca. 1.8–1.9, indicating that the DNA is sufficiently free of protein [20], and the concentration is determined by UV absorbance at 260 nm ( $\epsilon = 6600 \text{ M}^{-1} \text{ cm}^{-1}$ ) [21]. Electronic absorption spectra (200–700 nm) are carried out using 1 cm quartz cuvettes at 25 °C by fixing the concentration of ligand or complex ( $1.00 \times 10^{-3} \text{ mol L}^{-1}$ ), while gradually increasing the concentration of CT-DNA (0.00 to  $1.30 \times 10^{-4} \text{ mol L}^{-1}$ ). An equal amount of CT-DNA is added to both the compound solutions and the reference buffer solution to eliminate the absorbance of CT-DNA itself. The intrinsic binding constant  $K_b$  of the compound with CT-DNA is determined using the following equation (Eq. (1)) [20]:

$$[\text{DNA}]/(\epsilon_a - \epsilon_f) = [\text{DNA}]/(\epsilon_b - \epsilon_f) + 1/K_b(\epsilon_a - \epsilon_f) \quad (1)$$

where [DNA] is the concentration of CT-DNA in base pairs,  $\epsilon_a$  is the extinction coefficient observed for the  $A_{\text{obs}}/[\text{compound}]$  at the given DNA concentration,  $\epsilon_f$  is the extinction coefficient of the free compound

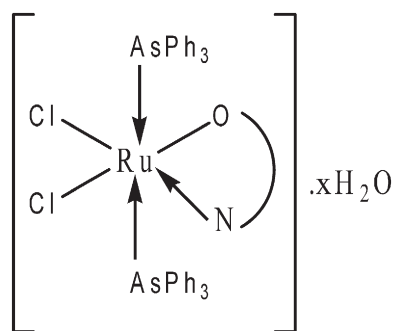


Fig. 1. Structure of Ru(III) complexes (1–3).

in solution and  $\epsilon_b$  is the extinction coefficient of the compound when fully bound to DNA. In plots of  $[\text{DNA}]/(\epsilon_a - \epsilon_f)$  versus [DNA],  $K_b$  is given by the ratio of the slope to the intercept.

### 2.4. Biological activity investigation

For this investigation the agar well diffusion method was applied [8, 22]. The antibacterial activities of the investigated compounds were tested against two local Gram positive bacterial species (*Bacillus cereus* and *Staphylococcus aureus*) and two local Gram negative bacterial species (*Escherichia coli* and *Klebsiella pneumoniae*) on nutrient agar

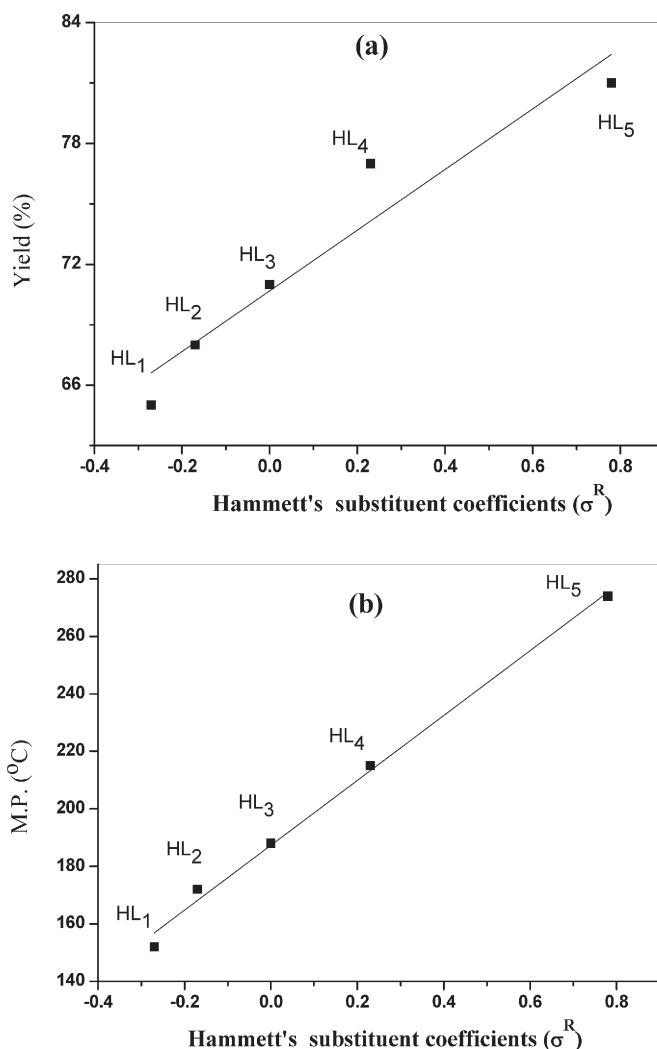


Fig. 2. The relation between Hammett's substitution coefficient ( $\sigma^R$ ) vs. (a) Yield (%) and (b) melting point (°C) of ligands (HL<sub>n</sub>).

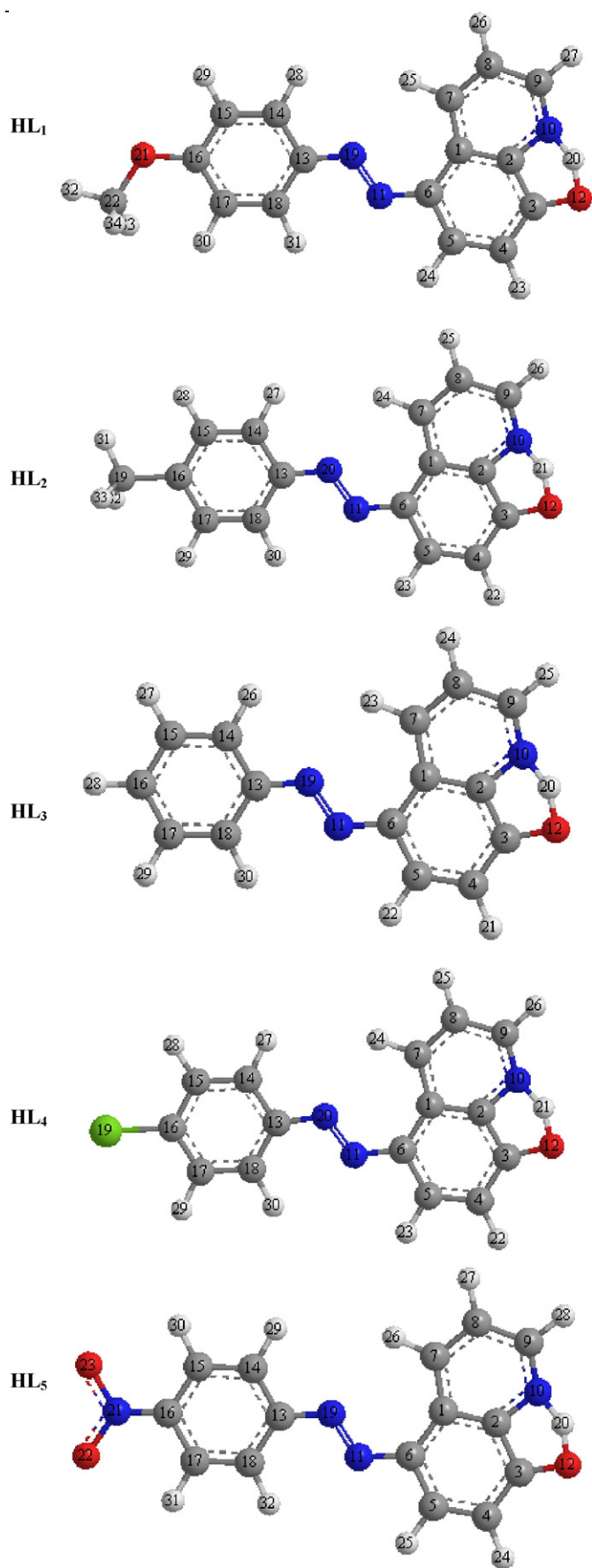


Fig. 3. Optimized structures of the ligands (HL<sub>n</sub>).

medium. Also, the antifungal activities were tested against four local fungal species (*Aspergillus niger*, *Alternaria alternata*, *Penicillium italicum* and *Fusarium oxysporium*) on DOX agar medium. The concentrations of

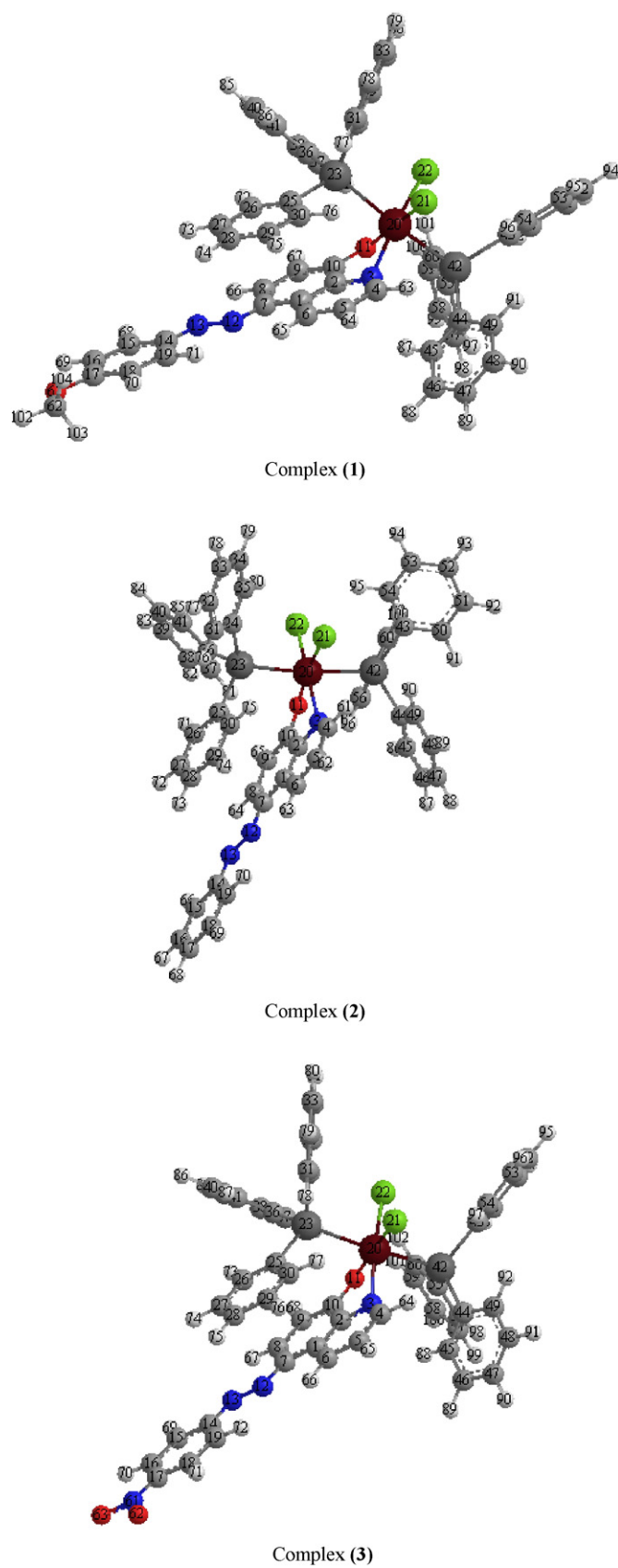


Fig. 4. Optimized structures of Ru(III) complexes (1–3).

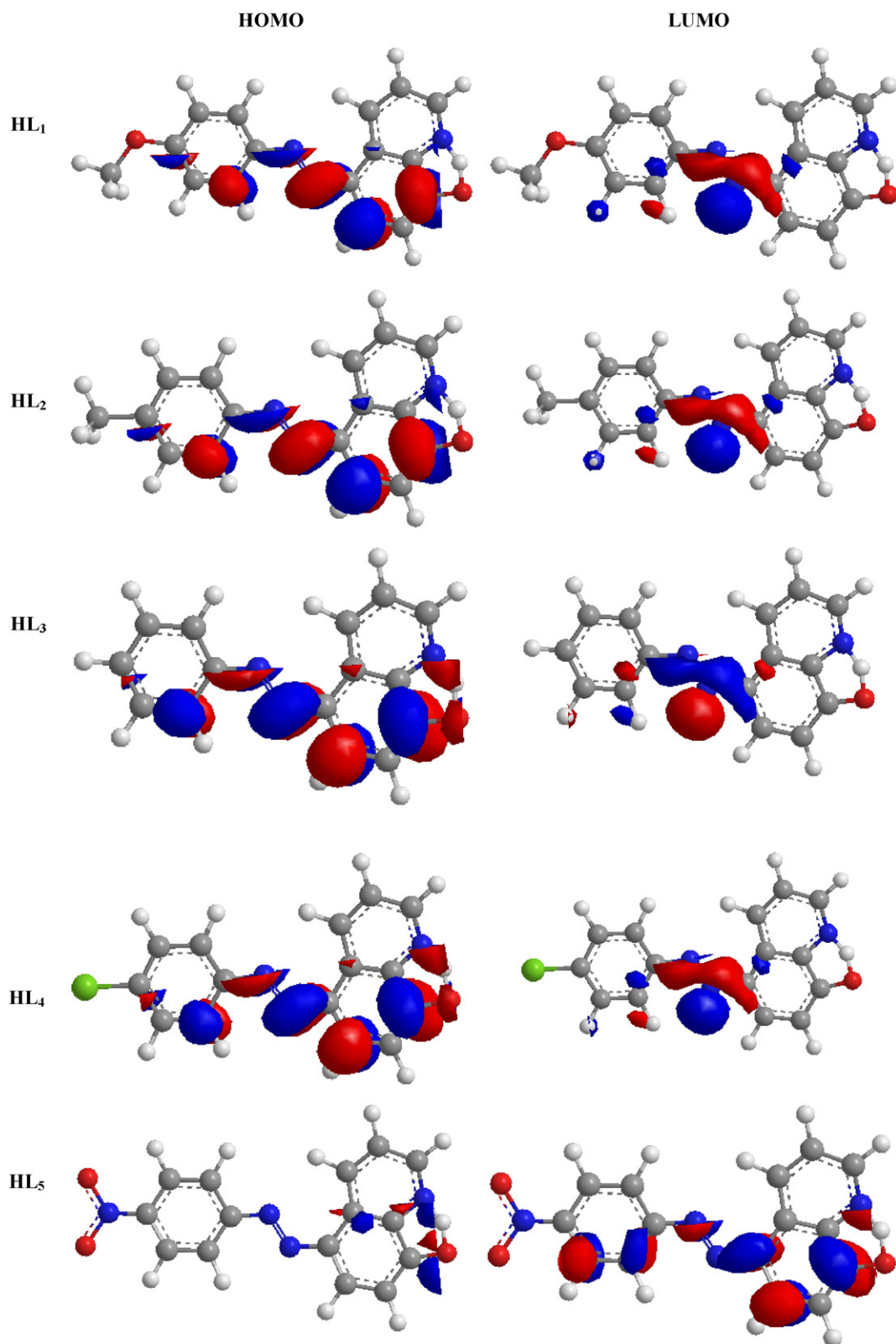


Fig. 5. HOMO and LUMO orbital of ligands (HL<sub>n</sub>).

each solution were 50, 100 and 150  $\mu\text{g/ml}$  in dimethyl formamide (DMF). By using a sterile cork borer (10 mm diameter), wells were made in agar medium plates previously seeded with the test microorganism. 200  $\mu\text{l}$  of each compound was applied in each well. The

agar plates were kept at 4  $^{\circ}\text{C}$  for at least 30 min to allow the diffusion of the compound to agar medium. The plates were then incubated at 37  $^{\circ}\text{C}$  and 30  $^{\circ}\text{C}$  for bacteria and fungi, respectively. The diameters of inhibition zone were determined after 24 h and 7 days for bacteria and

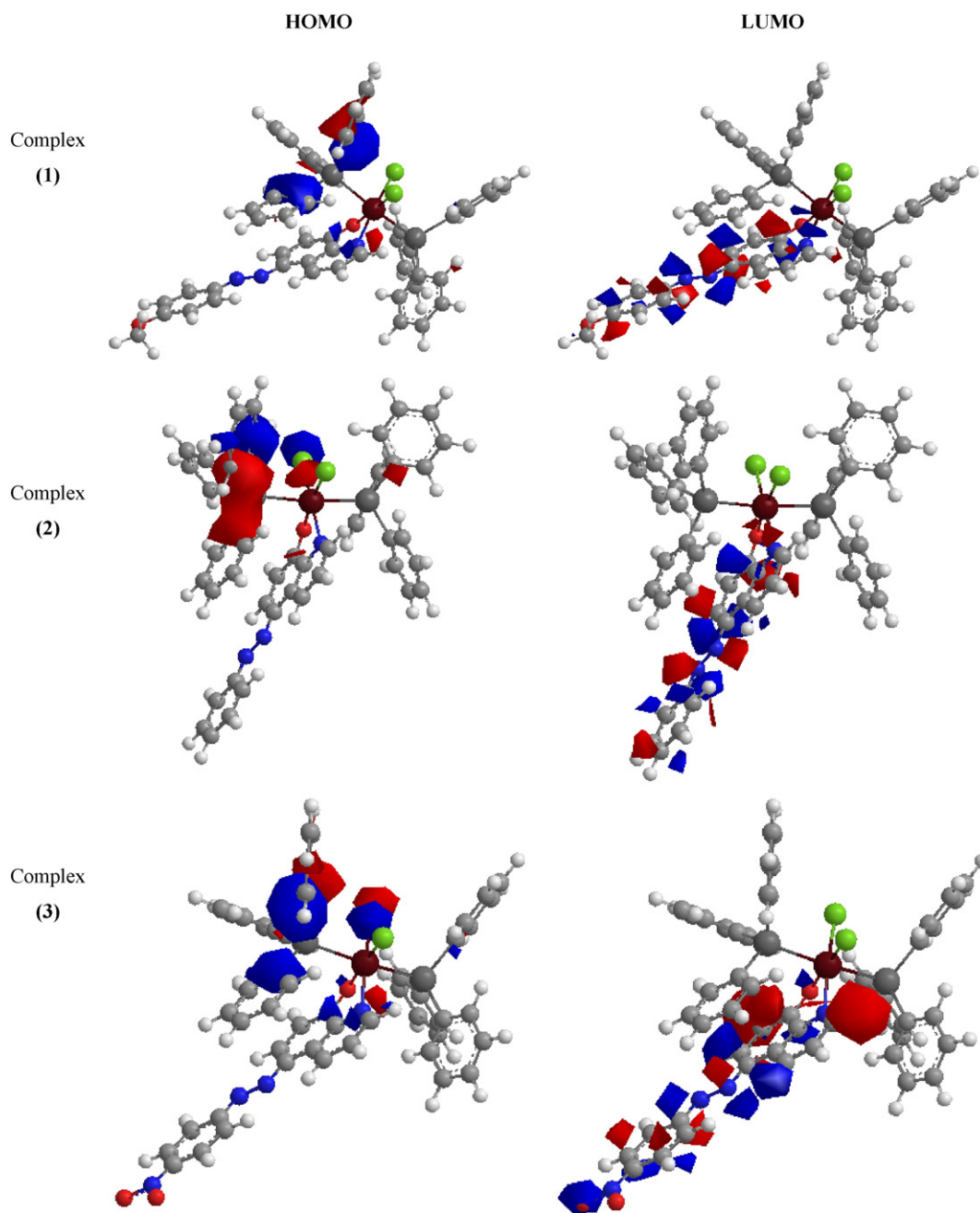


Fig. 6. HOMO and LUMO orbital of Ru(III) complexes (1–3).

fungi, respectively, taking into consideration the control values (DMF). Penicillin and miconazole were used as reference substances against bacteria and fungi, respectively.

### 2.5. Catalytic oxidation of alcohol by $[Ru(L_n)(AsPh_3)_2Cl_2] \cdot IO(OH)_5$

Oxidation reaction of cyclohexanol is studied using ruthenium complexes as catalysts and the cyclohexanol as substrate at a 1:200 M ratio. Cyclohexanol (2 mmol) is added to a solution of the catalyst  $[Ru(L_n)(AsPh_3)_2Cl_2] \cdot xH_2O$  (0.01 mmol) in 5 cm<sup>3</sup> dichloromethane and 2.5 cm<sup>3</sup> of acetonitrile with stirring. Periodic acid (5 mmol in 10 cm<sup>3</sup> H<sub>2</sub>O) is then added dropwise within 15 min and the reaction is ultrasonically irradiated for 15 min at room temperature. The mixture is reduced in vacuum and the residues are collected in diethyl ether, filtered through a bed of silica gel and dried over anhydrous MgSO<sub>4</sub>. The

carbonyl compounds formed are isolated and quantified as their 2,4-dinitrophenylhydrazone derivatives [23].

### 2.6. Analytical techniques

All the chemicals and solvents are purchased from Sigma-Aldrich Chemicals Company (USA) and used without further purification. CT-DNA was purchased from SRL (India). Double distilled water was used to prepare all buffer solutions.

Microanalytical data (C, H and N) are collected on Automatic Analyzer CHNS Vario ELIII, Germany. Spectroscopic data are obtained using the following instruments: IR spectra (KBr disks, 4000–400 cm<sup>-1</sup>) by Jasco FTIR-4100 spectrophotometer; the <sup>1</sup>H and <sup>13</sup>C NMR spectra by Bruker WP 300 MHz using DMSO-d<sub>6</sub> as a solvent containing TMS as the internal standard; UV-Visible spectra by Perkin-Elmer AA800

**Table 2**  
The calculated quantum chemical parameters for ligands (HL<sub>n</sub>).

Compound	E <sub>HOMO</sub> (eV)	E <sub>LUMO</sub> (eV)	E <sub>t</sub> (eV)	χ (eV)	η (eV)	σ (eV) <sup>-1</sup>	Pi (eV)	S (eV) <sup>-1</sup>	Ω (eV)	ΔN <sub>max</sub>
<i>HL<sub>1</sub></i>										
Form A	-4.694	-2.038	2.656	3.366	1.328	0.753	-3.366	0.377	4.266	2.535
Form A'	-7.593	-4.013	3.580	5.803	1.790	0.559	-5.803	0.279	9.406	3.242
Form B	-4.079	-1.695	2.386	2.887	1.192	0.839	-2.887	0.419	3.497	2.422
<i>HL<sub>2</sub></i>										
Form A	-4.897	-2.035	2.862	3.466	1.432	0.699	-3.466	0.349	4.197	2.421
Form A'	-7.593	-4.216	3.377	5.905	1.689	0.592	-5.905	0.296	10.324	3.497
Form B	-4.266	-1.689	2.576	2.978	1.288	0.776	-2.978	0.388	3.442	2.312
<i>HL<sub>3</sub></i>										
Form A	-5.021	-2.030	2.991	3.525	1.495	0.669	-3.525	0.334	4.156	2.358
Form A'	-7.592	-4.341	3.251	5.967	1.626	0.615	-5.967	0.308	10.950	3.671
Form B	-4.384	-1.684	2.696	3.034	1.349	0.741	-3.034	0.370	3.410	2.248
<i>HL<sub>4</sub></i>										
Form A	-4.615	-2.029	2.586	3.322	1.293	0.773	-3.322	0.387	4.267	2.569
Form A'	-7.590	-3.942	3.648	5.766	1.824	0.548	-5.766	0.274	9.114	3.161
Form B	-4.011	-1.684	2.327	2.847	1.164	0.859	-2.847	0.429	3.484	2.447
<i>HL<sub>5</sub></i>										
Form A	-6.381	-2.735	3.646	4.558	1.823	0.549	-4.558	0.274	5.698	2.500
Form A'	-7.601	-4.005	3.596	5.803	1.798	0.556	-5.803	0.278	9.365	3.228
Form B	-5.573	-2.438	3.135	4.006	1.567	0.638	-4.006	0.319	5.118	2.556

**Table 3**  
The calculated quantum chemical parameters for Ru(III) complexes (1–3).

Complex	E <sub>HOMO</sub> (eV)	E <sub>LUMO</sub> (eV)	E <sub>t</sub> (eV)	χ (eV)	η (eV)	σ (eV) <sup>-1</sup>	Pi (eV)	S (eV) <sup>-1</sup>	ω (eV)	ΔN <sub>max</sub>
(1)	-6.521	-4.262	2.259	5.392	1.130	0.885	-5.392	0.443	12.868	4.773
(2)	-7.593	-4.590	3.003	6.092	1.502	0.666	-6.092	0.333	12.35	4.057
(3)	-6.514	-6.023	0.491	6.269	0.246	4.073	-6.269	2.037	80.028	25.534

Numbers as given in Table 1.

**Table 4**  
Energy values obtained in docking calculations of ligands with receptor prostate cancer mutant 2q7k-hormone.

Compound	Est. free energy of binding (kcal/mol)	Est. inhibition constant, K <sub>i</sub> (μM)	Electrostatic energy (kcal/mol)	Total intercooled energy (kcal/mol)	Interact surface
HL <sub>1</sub>	-6.55	15.89	-0.07	-7.69	526.151
HL <sub>2</sub>	-7.56	2.89	-0.17	-8.93	514.724
HL <sub>3</sub>	-7.29	4.54	+0.00	-8.06	485.118
HL <sub>4</sub>	-7.41	3.71	-0.18	-8.19	519.253
HL <sub>5</sub>	-6.08	35.20	-0.16	-7.24	523.436

spectrophotometer Model AAS; mass spectra were recorded by the EI technique at 70 eV using MS-5988 GS-MS Hewlett-Packard. Thermal analysis of compounds are carried out using a Shimadzu thermogravimetric analyzer under nitrogen atmosphere with heating rate of 15 °C/min over a temperature range from room temperature up to 800 °C. Magnetic susceptibility measurements are determined at room temperature on a Johnson Matthey magnetic susceptibility balance using Hg[Co(SCN)<sub>4</sub>] as calibrant. Conductivity measurements of the complexes at 25 ± 1 °C are determined in DMF (10<sup>-3</sup> M) using conductivity/TDS meter model Lutron YK-22CT. The molecular structures of the investigated compounds are optimized by HF method with 3-21G basis set. The molecules were built with the Perkin Elmer ChemBio Draw and optimized using Perkin Elmer ChemBio3D software [24,25]. X-ray diffraction measurement (XRD) is recorded on X-ray diffractometer in the range of diffraction angle 2θ = 5–80°. This analysis is carried out using CuK<sub>α1</sub> radiation (λ = 1.540598 Å). The applied voltage and the tube current are 40 kV and 30 mA, respectively. The diffraction peaks

are indexed and the lattice parameters are determined with the aid of CRYSFIRE computer program [17].

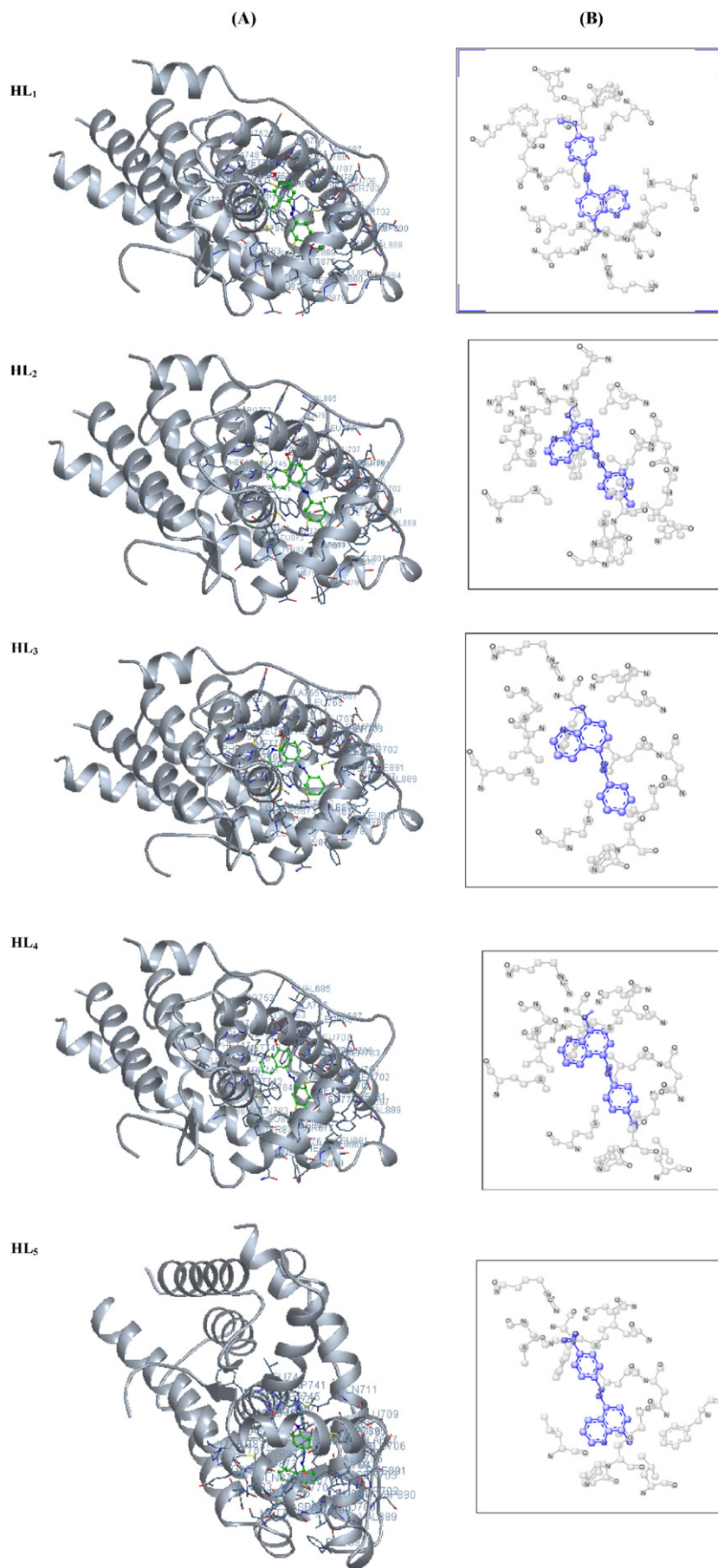
The docking process in which the ligand–protein interaction energies are calculated using a Docking Server [26,27]. The MMFF94 Force field was used for energy minimization of ligand molecule using Docking Server. Gasteiger partial charges were added to the ligand atoms. Non-polar hydrogen atoms were merged, and rotatable bonds were defined. Docking calculations were carried out on 2q7k-hormone protein model. Essential hydrogen atoms, Kollman united atom type charges, and solvation parameters were added with the aid of AutoDock tools [28]. Affinity (grid) maps of 20 × 20 × 20 Å grid points and 0.375 Å spacing were generated using the Autogrid program [29]. Auto Dock parameter set- and distance-dependent dielectric functions were used in the calculation of the van der Waals and the electrostatic terms, respectively.

### 3. Results and discussion

#### 3.1. The solid state structures

Hydrogen bonding represents one of the most versatile interactions that could be used for molecular recognition. The effects of protonation of the OH on the strength of the hydrogen bond of the ligand are simulated as a function of the length of the π-conjugated. It is known that 8-hydroxyquinoline, in solution, exists in a monomer dimer equilibrium. Our results suggest that in the monomeric form a strong intramolecular hydrogen bond is present. This is in agreement with a previous result [4,30]. The two such monomers lead to the dimer by formation of additional hydrogen bonding yielding the bifurcated hydrogen bonds and H–N–H nitrogen bridges (Scheme 1F).

**Fig. 7.** The ligands (HL<sub>n</sub>) (green in (A) and blue in (B)) in interaction with receptor prostate cancer mutant 2q7k-hormone. (For interpretation of the references to color in this figure legend, the reader is referred to the web version of this article).



In addition to the two bifurcated inter/intramolecular OH–N hydrogen bonds (Scheme 1C and D), two more intermolecular hydrogen bonding interactions are observed between nitrogen atom of azomethine group and phenolic hydroxyl hydrogen oxygen atom. This additional H-bonding does not influence the intramolecular distance which shows a band at a lower frequency than the intermolecular interaction. The reason for this behavior might be the additional H-bond which influences the hydrogen bonding ability of the hydroxyl group by electronic and/or steric factors. The overall structure of the dimer is close to planar with a slight shift of the two quinoline units from the plane. The dimer is able to dissociate, while the intermolecular interaction can only be broken if appropriate hydrogen bond acceptors are attached then acting as competitors to the quinoline nitrogen atoms.

The two hydroxyquinoline units of the dimer (Scheme 1F) are in one plane. The intermolecular (I) as well as intramolecular (II) hydrogen bonding occurs between the hydroxyl group and the quinoline nitrogen atom. The intermolecular hydrogen bond distance is shorter than the intramolecular one. This observation was also reported for other 8-hydroxyquinoline dimers and might be due to an unfavored small O–H–N angle for the intramolecular interaction [31,32].

As shown in Table 1, the values of yield (%) and melting point are related to the nature of the *p*-substituent as they increase according to the following order *p*-(NO<sub>2</sub> > Cl > H > CH<sub>3</sub> > OCH<sub>3</sub>). This can be attributed to the fact that the effective charge increased due to the electron withdrawing *p*-substituent (HL<sub>4</sub> and HL<sub>5</sub>) while it decreased by the electrons donating character of (HL<sub>1</sub> and HL<sub>2</sub>). This is in accordance with that expected from Hammett's constant ( $\sigma^R$ ) as shown in Fig. 2, correlate the yield (%) and/or melting point values with  $\sigma^R$  it is clear that all these values increase with increasing  $\sigma^R$ .

The measured molar conductance values of 10<sup>-3</sup> M solutions of the prepared Ru(III) complexes in DMF were found to be in the range of 26–50 Ω<sup>-1</sup> mol<sup>-1</sup> cm<sup>2</sup> which is in agreement with the non-electrolytic nature of the complexes. The non-electrolytic nature of the prepared complexes can be accounted by the deprotonation of the phenolic OH of the ligands when it is coordinated to Ru(III).

### 3.2. Geometrical structure of the ligands

The molecular structures of the ligands (HL<sub>*n*</sub>) and Ru(III) complexes are optimized by HF method with 3-21G basis set. Primary calculations reveal that the form (B) is more stable and reactive than forms (A) and (A') (Scheme 1). The calculated molecular structures for HL<sub>*n*</sub> and Ru(III) complexes are shown in Figs. 3 and 4. Selected geometric parameters bond lengths and bond angles of HL<sub>*n*</sub> and Ru(III) complexes are listed in Tables S1–S8 in the supplementary (azo form (B)).

Molecular structures (HOMO & LUMO) for HL<sub>*n*</sub> and Ru(III) complexes are presented in Figs. 5 and 6. The HOMO–LUMO energy gap ( $E_t$ ), which is an important stability index, is applied to develop theoretical models for explaining the structure and conformation barriers in many molecular systems. The smaller is the value of  $E_t$ , the more is the reactivity of the compound [33]. The calculated quantum chemical parameters are given in Tables 2 and 3. Additional parameters such as separation energies ( $E_t$ ), absolute electronegativities ( $\chi$ ), chemical potentials ( $\Pi$ ), absolute hardness ( $\eta$ ), absolute softness ( $\sigma$ ), global electrophilicity ( $\omega$ ), global softness ( $S$ ) and additional electronic charge ( $\Delta N_{\max}$ ) are calculated according to the following equations [34,35]:

$$E_t = E_{\text{LUMO}} - E_{\text{HOMO}} \quad (2)$$

$$\chi = \frac{-(E_{\text{HOMO}} + E_{\text{LUMO}})}{2} \quad (3)$$

$$\eta = \frac{E_{\text{LUMO}} - E_{\text{HOMO}}}{2} \quad (4)$$

$$\sigma = 1/\eta \quad (5)$$

$$\Pi = -\chi \quad (6)$$

$$S = \frac{1}{2\eta} \quad (7)$$

$$\omega = \Pi^2/2\eta \quad (8)$$

$$\Delta N_{\max} = -\Pi/\eta. \quad (9)$$

The azo form (B) is more reactive than azo form (A) (Scheme 1) as reflected from energy gap values (Table 2). The value of  $E_t$  for ligands HL<sub>1</sub>, HL<sub>2</sub>, HL<sub>3</sub>, HL<sub>4</sub> and HL<sub>5</sub> is found 2.386, 2.576, 2.696, 2.327 and 3.135 eV, respectively. The value of  $E_t$  for Ru(III) complexes (1–3) is found 2.259, 3.003 and 0.491 eV, respectively. It was found that the complex (3) is more stable than the other complexes.

### 3.3. Molecular docking study

The molecular docking is a key tool in computer drug design [26]. The focus of molecular docking is to simulate the molecular recognition process. Molecular docking aims to achieve an optimized conformation for both the protein and drug with relative orientation between them such that the free energy of the overall system is minimized [27].

The results of molecular docking between ligands (HL<sub>*n*</sub>) and receptor of prostate cancer mutant 2q7k-hormone showed a possible arrangement between ligands and receptor (2q7k). A docking study showing a favorable interaction between ligands and the receptor (2q7k) and the calculated energy are listed in Table 4 and Fig. 7. 2D plot curves of docking with ligands are shown in Fig. 8. This interaction could activate apoptosis in cancer cell energy of interactions with ligands. Binding energies are the most widely used mode of measuring binding affinity of ligands. Thus, decrease in binding energy due to mutation will increase the binding affinity of the ligands toward the receptor.

### 3.4. Mass spectra

The electron impact mass spectrum of ligand (HL<sub>3</sub>) is recorded and investigated at 70 eV of electron energy. It is obvious that the molecular ion peaks are in good agreement with their suggested empirical formula as indicated from elemental analysis (Table 1). The mass spectrum fragmentation mode of ligand (HL<sub>3</sub>) shows the exact mass of 249 corresponding to the formula C<sub>15</sub>H<sub>11</sub>N<sub>3</sub>O (Fig. 9). The ion of *m/z* = 249 undergoes fragmentation to a stable peak at *m/z* = 172 by losing C<sub>6</sub>H<sub>5</sub> atoms (structure I) as shown in Scheme 2. The loss of N<sub>2</sub> leads to the fragmentation with *m/z* = 144 (structure II). The loss of CHO atoms leads to the fragmentation with *m/z* = 115 (structure III). A breakdown of the backbone of HL<sub>3</sub> ligand gives the fragment (IV).

### 3.5. X-ray diffraction analysis

Single crystals of the ligands and their complexes could not be prepared to get the XRD and hence the powder diffraction data were obtained for structural characterization. Structure determination by X-ray powder diffraction data has gone through a recent surge since it has become important to get to the structural information of materials, which do not yield good quality single crystals.

The X-ray diffraction (XRD) patterns of HL<sub>3</sub> ligand and its complex (2) in powder form are shown in Figs. 10 and 11. The XRD patterns show that the ligand (HL<sub>3</sub>) has a polycrystalline nature and complex (2) is completely amorphous. The calculated crystal system of HL<sub>3</sub> ligand is found to be monoclinic with space group P21/A. The estimated lattice parameters are found to be 20.4710 Å, 18.8150 Å, 19.9590 Å, 90.0°, 92.7° and 90.0° for *a*, *b*, *c*,  $\alpha$ ,  $\beta$  and  $\gamma$ , respectively. The inter-planar spacing (*d*) and Miller indices (*hkl*) which are estimated by CRYSFIRE are listed in Table 5. The average crystallite size (*S*) is calculated according to Scherer's

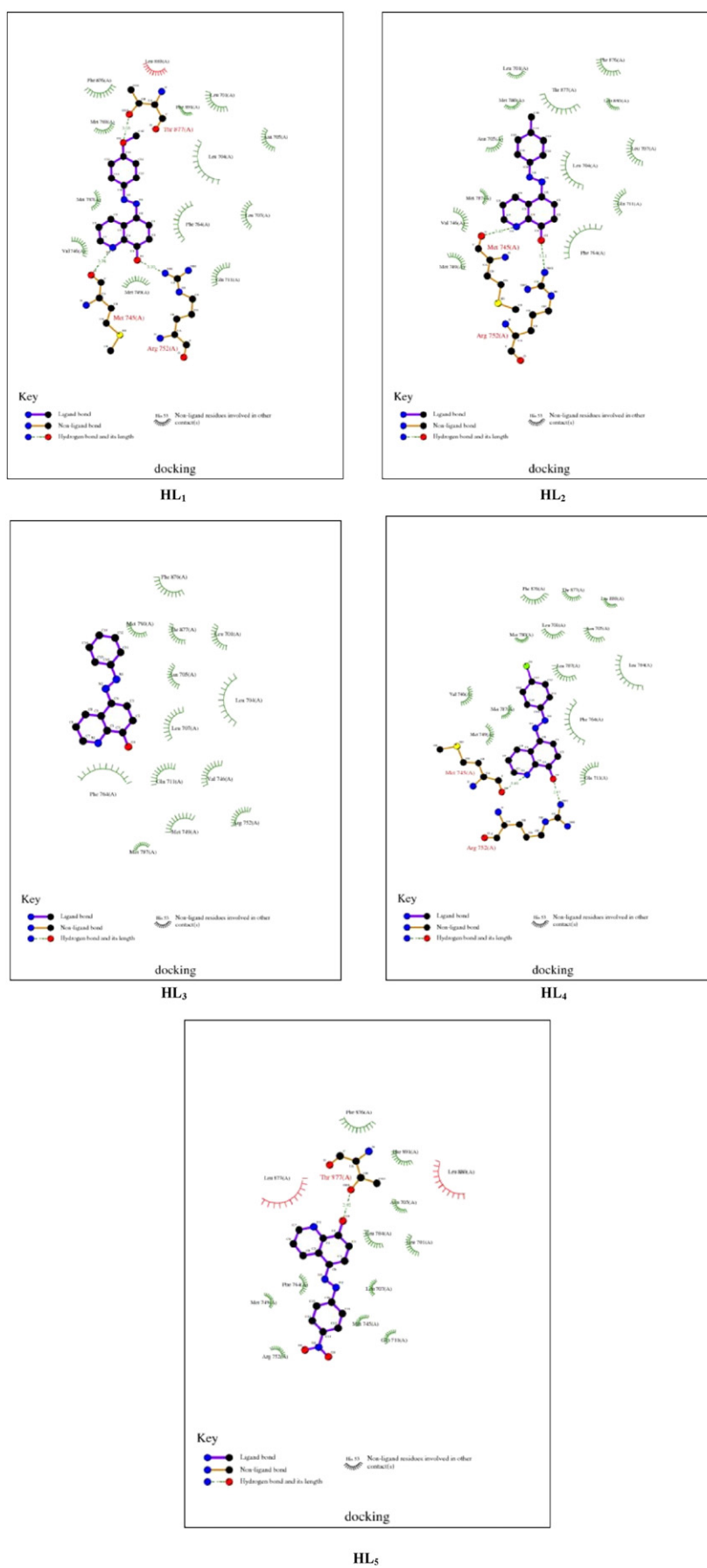


Fig. 8. 2D plot of interaction between ligands (HL<sub>n</sub>) and receptor of prostate cancer mutant 2q7k-hormone.

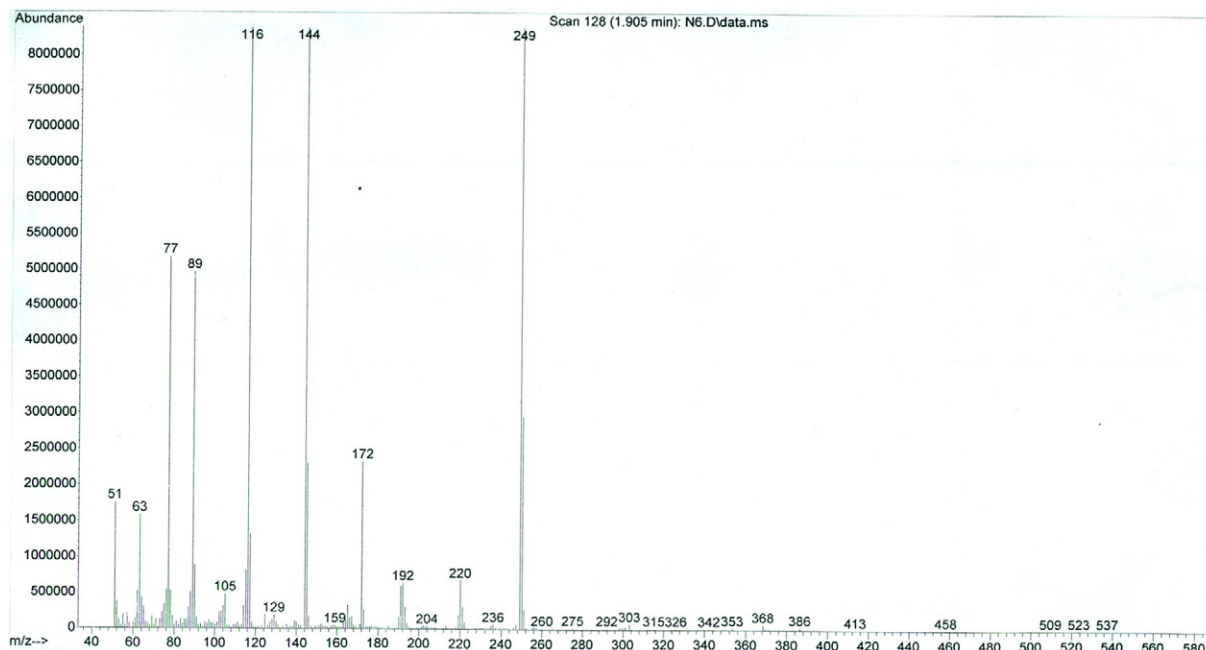


Fig. 9. Mass spectrum of HL<sub>3</sub> ligand.

equation [17,36] as follows:

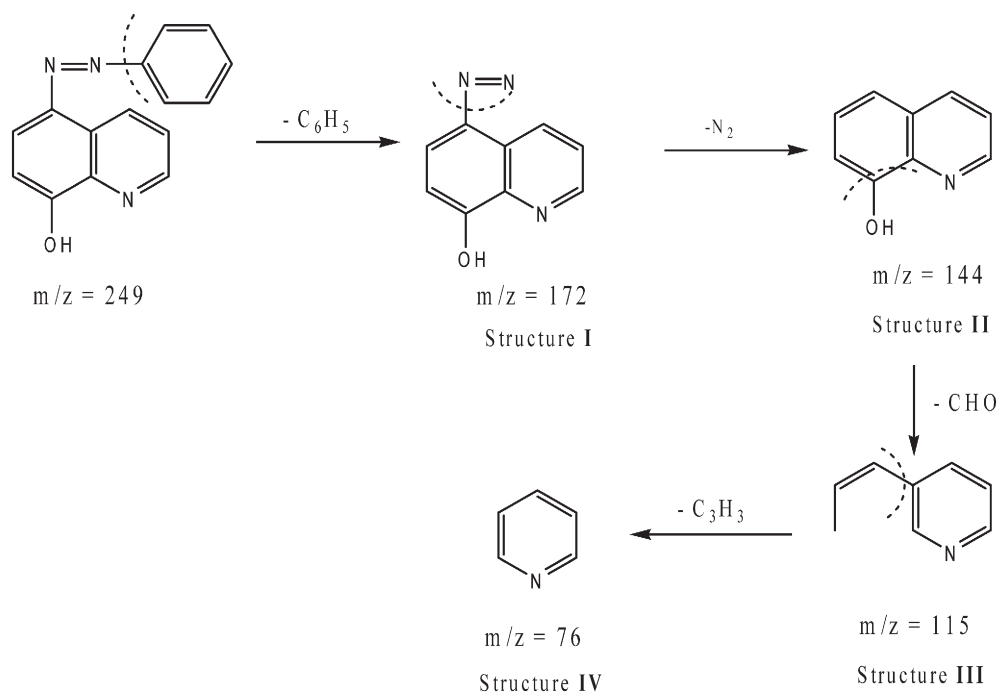
$$S = \frac{0.95\lambda}{\psi \cos\theta} \quad (10)$$

where  $\psi$  is the width measured in radians of the half-maximum peak intensity,  $\lambda$  is the X-ray wavelength and  $\theta$  is the Bragg's angle. The estimated crystallite size ( $S$ ) of HL<sub>3</sub> ligand is found to be about 24.3 nm.

### 3.6. <sup>1</sup>H and <sup>13</sup>C NMR spectra

The <sup>1</sup>H and <sup>13</sup>C NMR spectra of (HL<sub>n</sub>) were recorded in dimethylsulphoxide (DMSO-d<sub>6</sub>) solution using tetramethylsilane (TMS) as internal standard.

El-Sonbati and coworkers [17,18,37] investigated the NMR spectra of quinoline and its derivatives with various transition metal salts. The <sup>1</sup>H NMR spectra of quinoline and benzene rings appeared in the range of 7.01–8.25 ppm. For the HL<sub>1</sub> has a singlet observed at 3.88 ppm is assigned to OCH<sub>3</sub> protons (the integration curve shows 3 protons).



Scheme 2. Fragmentation patterns of HL<sub>3</sub> ligand.

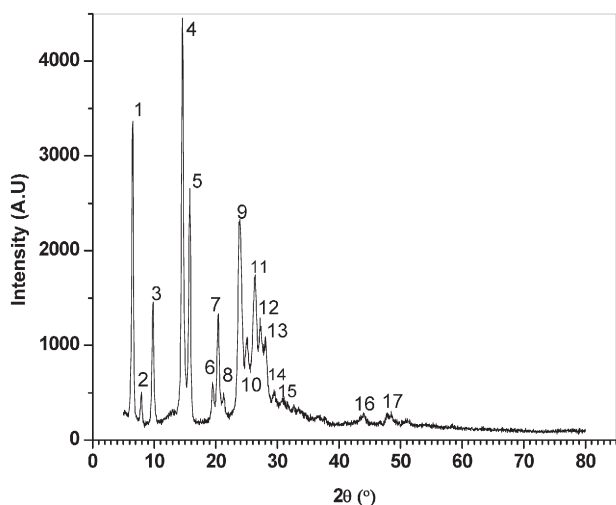


Fig. 10. X-ray diffraction pattern of HL<sub>3</sub> in powder form.

Also HL<sub>2</sub> has a singlet at 3.76 ppm which is assigned to the CH<sub>3</sub> protons. The <sup>1</sup>H NMR spectra show two singlets for C<sub>8</sub>-OH at ~9.55–10.30 ppm and HCN at ~9.09–9.30 ppm, favoring formation of an intramolecular hydrogen bond with the azomethine group. Electron-withdrawing substituents reduce the intramolecular hydrogen bond as indicated by the marked shift of the hydroxyl signal to higher field in the *p*-NO<sub>2</sub> compound. Electron-donating substituents give the opposite effect, arising from the increasing basicity of the azo-nitrogen. The broad signals due to the C<sub>8</sub>-OH protons at ~9.55–10.30 ppm are not affected by dilution but rapidly exchange in the presence of D<sub>2</sub>O. The weak and broad band of hydroxyl proton was most probably resulted from intra-H-bonding of OH proton with N atom of azomethine quinoline group. The weakening and broadening of this type of proton signal might be caused by dimer formation between two hydroxyl quinoline groups of two different molecules as mentioned by Albrecht et al. [38] and El-Sonbati et al. [18,37]. HL<sub>*n*</sub> ligands may exist in two possible tautomeric forms, namely azo and hydrazone forms as depicted in Fig. 12. Diab et al. [3,4] reported the structures of some quinoline azodyes and pointed out that the azo form existed in the crystal form. Important structural information about HL<sub>*n*</sub> was obtained from the <sup>1</sup>H and <sup>13</sup>C NMR spectra. In the <sup>13</sup>C NMR, there is no detected signal for the carbon of carbonyl group (CO) at quinoline ring for the hydrazone form. The signal for the N-H proton of HL<sub>*n*</sub> for the hydrazone form was not observed in DMSO-*d*<sub>6</sub>.

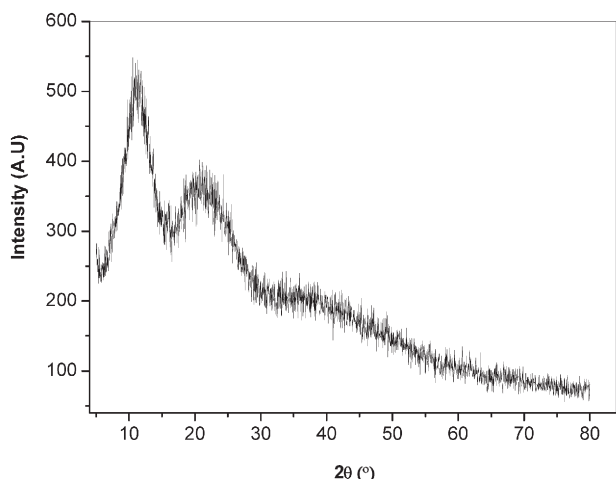


Fig. 11. X-ray diffraction pattern of complex (2) in powder form.

Table 5  
Crystallographic data of HL<sub>3</sub>.

Peak no.	2θ <sub>obs.</sub> (°)	d <sub>obs.</sub> (Å)	d <sub>cal.</sub> (Å)	(hkl)
1	6.514	13.56162	13.70641	0 1 1
2	7.917	11.16377	11.21252	1 1 1
3	9.788	9.030481	8.988331	$\bar{2}$ 1 0
4	14.586	6.070134	6.070134	$\bar{1}$ 1 3
5	15.772	5.614431	5.606259	2 2 2
6	19.490	4.5526	4.563389	0 3 3
7	20.388	4.354438	4.344614	4 1 2
8	21.288	4.170547	4.170547	3 2 3
9	23.871	3.724855	3.730266	$\bar{4}$ 3 2
10	24.110	3.689176	3.692713	$\bar{2}$ 3 4
11	25.052	3.553044	3.562905	$\bar{5}$ 2 2
12	26.359	3.378509	3.385934	$\bar{3}$ 4 3
13	27.205	3.276478	3.275085	0 5 3
14	28.082	3.175185	3.176495	3 2 5
15	29.584	3.017235	3.0196	3 4 4
16	44.022	2.055778	2.055778	$\bar{7}$ 6 3
17	47.760	1.902915	1.902915	$\bar{5}$ 8 4

### 3.7. IR spectra

El-Sonbati, Bardez and coworkers [18,39,40] have characterized the steady-state spectroscopy of 8-hydroxyquinoline which forms a very stable hydrogen bonded dimer whose structure is given in Scheme 1 along with that for the tautomer. Scheme 1D and E shows the structures of both the dimer and the tautomer. The infrared spectra of the O-H stretching transition of the dimers indicate tremendous stability. Although the vibrational spectra of hydrogen-bonded molecules are often very broad, the O-H stretching transition of 8-hydroxyquinoline dimers has a width of only about 25 cm<sup>-1</sup>, indicating that the dimers are well-defined with stable structures. Typically, aromatic systems that form hydrogen-bonded dimers in the ground state show new features corresponding to the dimer and an associated isosbestic point as a function of concentration. These features do not appear in the 8-hydroxyquinoline spectra because, even at very low concentration, dimers are the dominant species.

The 8-hydroxyquinoline exists, in solution, in monomer dimer equilibrium. The results of this study indicate that, in the monomeric form, a strong intramolecular hydrogen bond is present. This is in agreement with previous results [41]. Two such monomers lead to the dimer by forming additional hydrogen bonding yielding the bifurcated hydrogen bonds and H-N-H nitrogen bridges (Scheme 1F).

HL<sub>*n*</sub> ligands exist as a five-membered chelate skeleton with hydrogen bonding classified into two types:

- An intramolecular hydrogen bond O-H...N (Scheme 1B) is found between hydrogen of (C<sub>8</sub>-OH) and nitrogen of azomethine group (CN<sub>*py*</sub>).
- An intermolecular hydrogen bonding (O-H...O) (Scheme 1C) resulting from the C<sub>8</sub>-OH group itself and/or C<sub>8</sub>-OH with CN between two molecules and O-H...N (Scheme 1D). The strong 950 cm<sup>-1</sup> band indicates the existence of this ligand in a dimer skeleton, associated structure through intermolecular hydrogen bonds (Scheme 1).

IR spectra of the ligands (HL<sub>*n*</sub>) exhibit a medium to strong band in the range of 1500–1504 cm<sup>-1</sup> which could be assigned to ν<sub>NN</sub> stretching vibration (Table 6) [6,10]. It was found that the -OH in hydroxy compounds suffered a blue shift when the OH group is involved in a hydrogen bond [17,42].

In IR spectra of HL<sub>*n*</sub>, there are two bands in the range of 3266–3315 and 1570–1590 cm<sup>-1</sup> for stretching OH of quinoline at C<sub>8</sub>-position and CN<sub>*quin*</sub>. (nitrogen atom of azomethine of quinoline group), respectively. The effect of intramolecular H-bonding between the OH hydrogen at C<sub>8</sub>-position of quinoline and the N atom of the quinoline ring (Scheme 1)

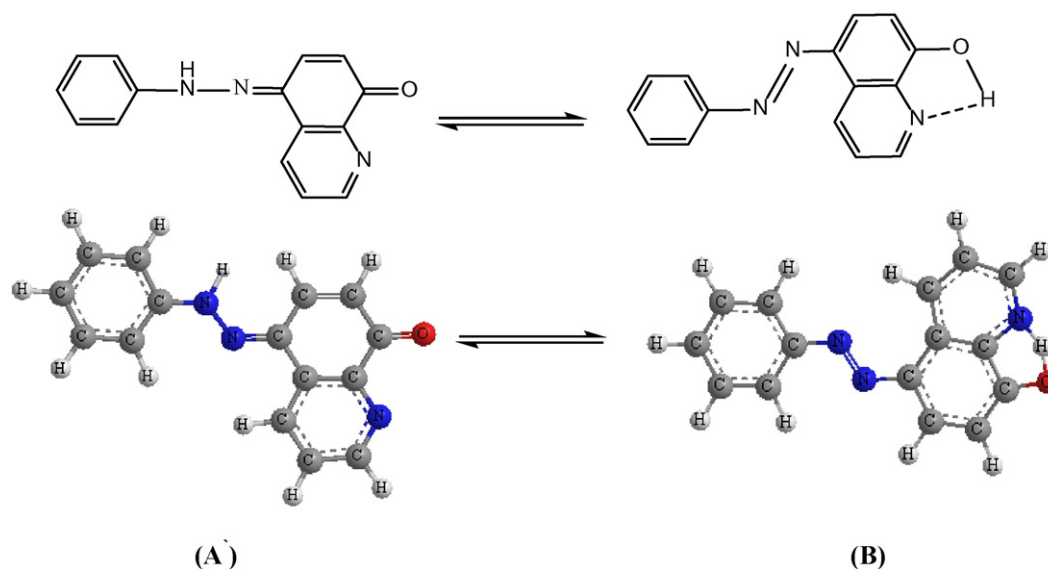


Fig. 12. Structure of azo and hydrazone forms of HL<sub>3</sub> ligand.

can be seen through decreasing in wavenumber. Teimouri et al. [43] observed the similar OH stretching frequency of hydroxyquinoline at  $3535\text{ cm}^{-1}$  and Krishnakumar and Ramasamy [44] found the same OH band of hydroxyquinoline at  $3420\text{ cm}^{-1}$ . The aromatic C–H bands was observed at  $3000\text{--}3120\text{ cm}^{-1}$  as used and methyl C–H vibration of methoxy group was observed at  $2990\text{--}2850\text{ cm}^{-1}$ . This indicates that the C–H vibrations appeared at relatively higher frequency than the normal aliphatic C–H vibration of paraffines as a result of stronger C–H bonds in methoxy group caused by oxygen atom making C atoms more electropositive. The absorption due to azo group in carbon 5 of the 8-hydroxyquinoline ring remains unaltered in the spectra of the complexes indicating the non-involvement of the azo group in coordination. IR spectra show that the ligands (HL<sub>n</sub>) act as a monobasic bidentate ligand by coordinating via the nitrogen atom of azomethine and oxygen atom of the deprotonated –OH group of 8-hydroxyquinoline, thereby forming a five-membered chelating ring and concomitant formation of an intramolecular hydrogen bond.

It was further observed that, the bands due to O–H–N disappeared and the stretching frequencies of  $\nu(\text{C}=\text{O})$  were shifted to higher frequencies  $1240\text{--}1270\text{ cm}^{-1}$  in the spectra of all complexes, these results indicate a phenomenon of deprotonation of hydroxy group and the coordination of the phenolic oxygen to the ruthenium centre. These results are supported by the appearance of new bands in the range of  $526\text{--}574\text{ cm}^{-1}$  and  $468\text{--}472\text{ cm}^{-1}$  can be attributable to  $\nu(\text{Ru}=\text{O})$  and  $\nu(\text{Ru}=\text{N})$  stretching bands, respectively [16,45]. In addition to the above, three strong bands were also observed in the spectra of all complexes near  $649$ ,  $686$  and  $736\text{ cm}^{-1}$  which are attributable to the coordinated triphenylarsine.

The mode of coordination is also confirmed from the  $^1\text{H}$  NMR data in which the OH signal disappeared. This is accompanied by disappearance

of the hydrogen bond and displacement of a proton as well as the coordination through the oxygen of hydroxyl.

### 3.8. Magnetic moment and electronic spectra

The magnetic susceptibility measurements at room temperature show that the magnetic moments of ruthenium complexes lie in the range  $1.7\text{--}2.1\text{ BM}$ , corresponding to one unpaired electron. It is inferred from the values that ruthenium is in the +3 oxidation state. HL<sub>n</sub> ligands exhibit bands at  $\sim 32,500\text{ cm}^{-1}$  (CN) ( $\pi\text{--}\pi^*$ ),  $33,450\text{ cm}^{-1}$  (H-bonding and association),  $\sim 40,040\text{ cm}^{-1}$  (phenyl) ( $\text{Ph}=\text{Ph}^*$ ,  $\pi\text{--}\pi^*$ ) [39,46] and  $\sim 29,340\text{ cm}^{-1}$ , and transition of phenyl rings overlapped by composite broad ( $\pi\text{--}\pi^*$ ), of azo structure.

The electronic spectra of all complexes are recorded in dimethylformamide solvent in the range of  $33,333\text{--}14,285\text{ cm}^{-1}$  (Fig. 13). The spectral data are listed in Table 7. The ground state of ruthenium (III) ion ( $t_{2g}^5\text{--}e_g^2$  configuration) is  $^2T_{1g}$  and the first excited doublet levels, in order of increasing energy, are  $^2A_{2g}$  and  $^2T_{1g}$  arising from  $t_{2g}^4 e_g^1$  configuration. Bands that are observed in  $22,222\text{--}14,285\text{ cm}^{-1}$  regions have been assigned to d–d transitions, while bands in the  $28,570\text{--}20,830\text{ cm}^{-1}$  regions are assigned to charge transfer transitions. These

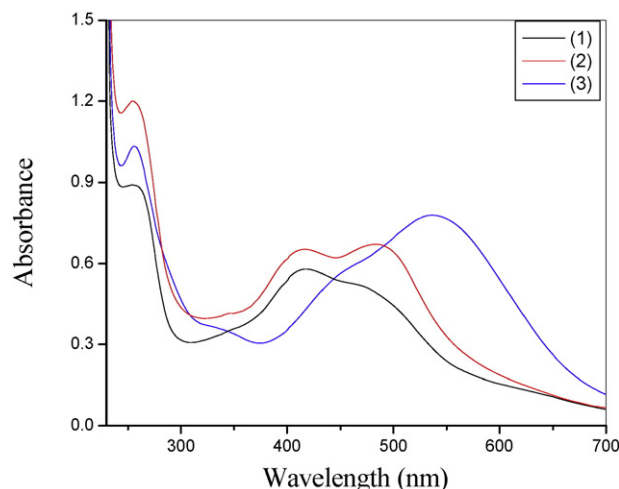


Fig. 13. Electronic spectra of the Ru(III) complexes (1–3).

Table 6  
IR data ( $\text{cm}^{-1}$ ) of free ligands (HL<sub>n</sub>) and Ru(III) complexes (1–3).

Compound <sup>a</sup>	$\nu(\text{OH})$	$\nu(\text{NN})$	$\nu(\text{Ru}=\text{O})$	$\nu(\text{Ru}=\text{N})$
HL <sub>1</sub>	3315	1500	–	–
(1)	–	1498	568	470
HL <sub>2</sub>	3266	1500	–	–
HL <sub>3</sub>	3272	1504	–	–
(2)	–	1500	574	468
HL <sub>4</sub>	3284	1502	–	–
HL <sub>5</sub>	3278	1504	–	–
(3)	–	1504	526	472

<sup>a</sup> Numbers as given in Table 1.

**Table 7**  
Electronic spectral data for the Ru(III) complexes (1–3).

Complex <sup>a</sup>	d–d transition (cm <sup>-1</sup> )	Charge transfer (cm <sup>-1</sup> )
(1)	21,740–16,666	28,570–21,740
(2)	22,222–16,666	28,570–22,222
(3)	20,830–14,285	26,315–20,830

<sup>a</sup> Numbers as given in Table 1.

results are found to be in conformity with the assignments made for similar ruthenium (III) complexes [20].

### 3.9. Thermal analysis

Thermal analysis plays an important role in determining thermal stability of the organic material [47–49].

The TGA curves for the ligands (HL<sub>n</sub>) and Ru(III) complexes (1–3) are shown in Figs. 14 and 15. It is clear that the change of substituent affects the thermal properties of the ligands. The TGA curves for HL<sub>1</sub> and HL<sub>4</sub> show three steps of the loss of masses, while for HL<sub>2</sub>, HL<sub>3</sub> and HL<sub>5</sub> show two steps. Also the complexes show two steps of the loss of masses. The first and second stages of decomposition in the range ~60–700 °C for Ru(III) complexes can be attributed to loss of a part of the ligand. The third stage of decomposition of the rest of the ligand leaving RuO<sub>2</sub> residue. The temperature intervals and the percentage of loss of masses are listed in Table 8.

### 3.10. Calculation of activation thermodynamic parameters

The thermodynamic activation parameters of decomposition processes of the ligands (HL<sub>n</sub>) and Ru(III) complexes (1–3) namely activation energy (E<sub>a</sub>), enthalpy (ΔH<sup>\*</sup>), entropy (ΔS<sup>\*</sup>), and Gibbs free energy change of the decomposition (ΔG<sup>\*</sup>) are evaluated graphically by employing the Coast–Redfern [50] and Horowitz–Metzger [51] methods.

#### 3.10.1. Coast–Redfern equation

The Coast–Redfern equation, which is a typical integral method, can represent as:

$$\int_0^{\alpha} \frac{dx}{(1-\alpha)^n} = \frac{A}{\phi} \int_{T_1}^{T_2} \exp\left(-\frac{E_a}{RT}\right) dt. \quad (11)$$

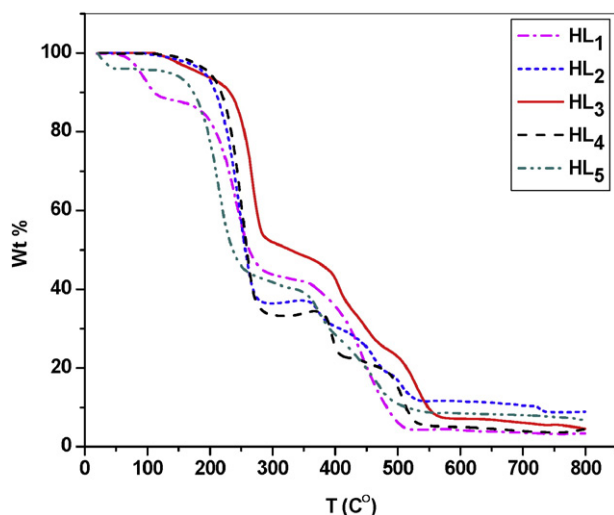
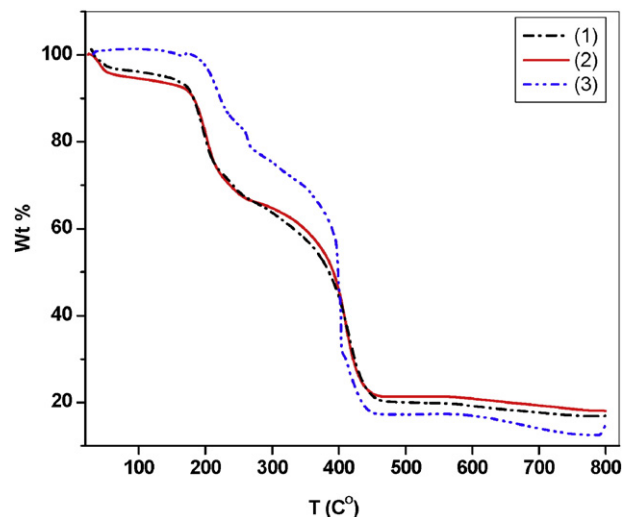
Fig. 14. TGA curves of ligands (HL<sub>n</sub>).

Fig. 15. TGA curves of Ru(III) complexes (1–3).

For convenience of integration, the lower limit T<sub>1</sub> usually taken as zero. This equation on integration gives:

$$\ln\left[-\frac{\ln(1-\alpha)}{T^2}\right] = -\frac{E_a}{RT} + \left[\frac{AR}{\phi E_a}\right]. \quad (12)$$

A plot of left-hand side (LHS) against 1/T was drawn (Figs. 16 and 17). E<sub>a</sub> is the energy of activation in J mol<sup>-1</sup> and calculated from the slope and A in (s<sup>-1</sup>) from the interception value. The entropy of activation (ΔS<sup>\*</sup>) in (J mol<sup>-1</sup> K<sup>-1</sup>) calculated by using the equation:

$$\Delta S^* = 2.303 \left[ \log\left(\frac{Ah}{k_B T_S}\right) \right] R \quad (13)$$

**Table 8**The thermal analysis data for ligands (HL<sub>n</sub>) and Ru(III) complexes (1–3).

Compound <sup>a</sup>	Temp. range (°C)	Found mass loss (calc.) %	Assignment
HL <sub>1</sub>	50–136	11.8 (11.11)	Loss of OCH <sub>3</sub>
	136–300	44.5 (43.01)	Loss of C <sub>6</sub> H <sub>4</sub> N <sub>2</sub> O
	300–800	40.3 (41.57)	Loss of C <sub>8</sub> H <sub>6</sub> N
	>800	3.39 (4.30)	Loss of C atom
HL <sub>2</sub>	90–300	63.64 (65.40)	Loss of C <sub>9</sub> H <sub>6</sub> N <sub>3</sub> O
	300–800	27.5 (25.48)	Loss of C <sub>5</sub> H <sub>7</sub>
	>800	8.86 (4.56)	Loss of C atom
HL <sub>3</sub>	100–300	48.10 (48.59)	Loss of C <sub>6</sub> H <sub>5</sub> N <sub>2</sub> O
	300–800	47.40 (46.59)	Loss of C <sub>8</sub> H <sub>6</sub> N
	>800	4.50 (4.82)	Loss of C atom
HL <sub>4</sub>	110–300	66.55 (67.55)	Loss of C <sub>10</sub> H <sub>6</sub> NOCl
	300–430	10.96 (9.88)	Loss of N <sub>2</sub>
	430–800	18.04 (18.34)	Loss of C <sub>4</sub> H <sub>4</sub>
	>800	4.45 (4.23)	Loss of C atom
HL <sub>5</sub>	120–270	56.51 (56.46)	Loss of C <sub>6</sub> H <sub>4</sub> N <sub>3</sub> O <sub>3</sub>
	270–800	36.79 (39.46)	Loss of C <sub>8</sub> H <sub>6</sub> N
	>800	6.7 (4.08)	Loss of C atom
(1)	30–70	3.32 (3.28)	Loss of 2H <sub>2</sub> O
	70–270	30.32 (30.32)	Loss of C <sub>20</sub> H <sub>18</sub> As
	270–800	49.45 (49.91)	Loss of C <sub>28</sub> H <sub>24</sub> N <sub>3</sub> Cl <sub>2</sub> AS
	>800	16.91 (16.49)	Loss of 4C + RuO <sub>2</sub>
(2)	24–60	4.4 (3.37)	Loss of 2H <sub>2</sub> O
	60–270	29.3 (28.65)	Loss of C <sub>18</sub> H <sub>15</sub> As
	270–800	48.26 (51.40)	Loss of C <sub>28</sub> H <sub>25</sub> N <sub>3</sub> Cl <sub>2</sub> AS
	>800	18.04 (18.08)	Loss of 5C + RuO <sub>2</sub>
(3)	31–350	30.6 (30.64)	Loss of C <sub>20</sub> H <sub>15</sub> As
	350–800	56.82 (58.49)	Loss of C <sub>31</sub> H <sub>24</sub> N <sub>4</sub> O <sub>2</sub> Cl <sub>2</sub> AS
	>800	12.58 (12.36)	Loss of RuO <sub>2</sub>

<sup>a</sup> Numbers as given in Table 1.

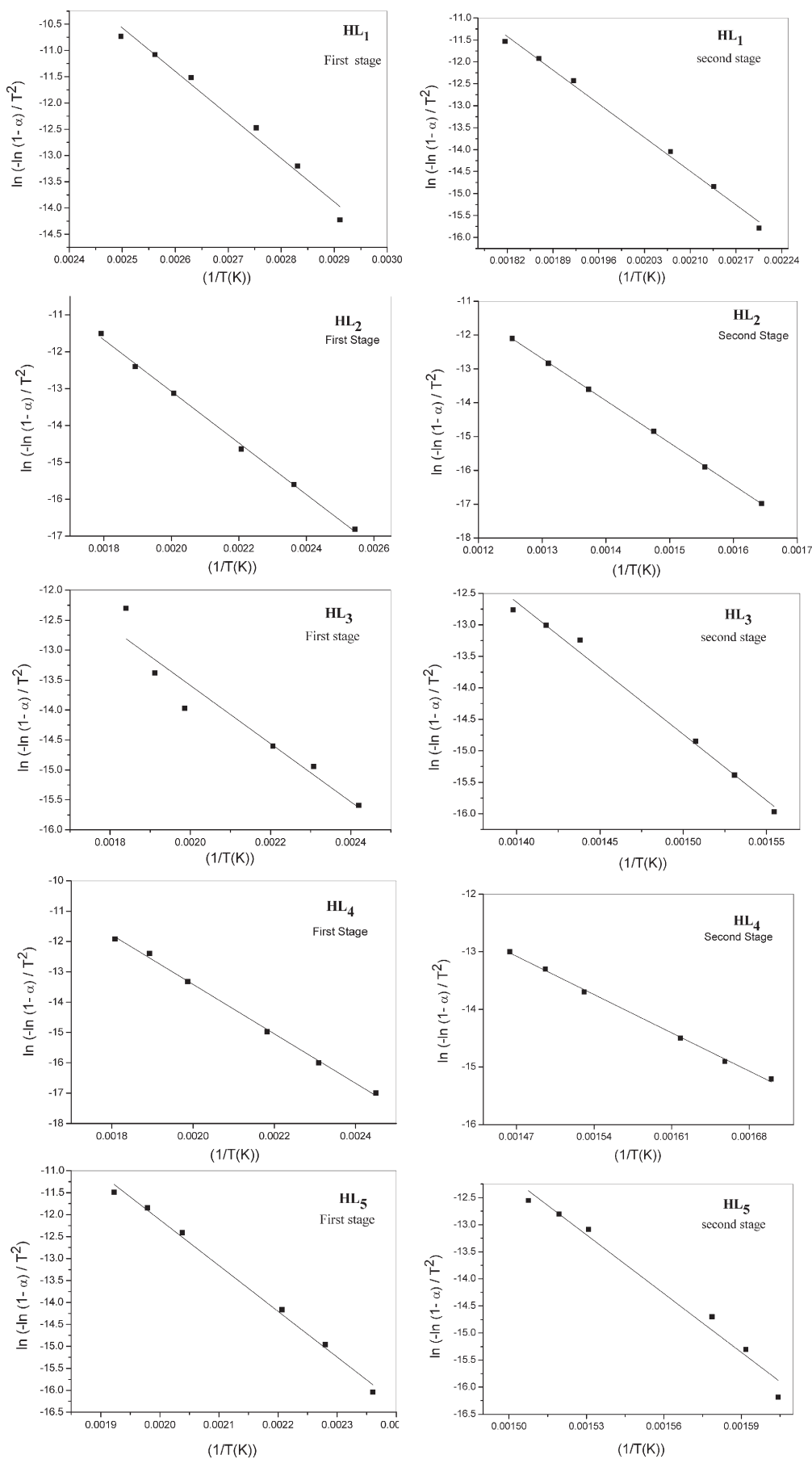


Fig. 16. Coats-Redfern (CR) of the ligands (HL<sub>n</sub>).

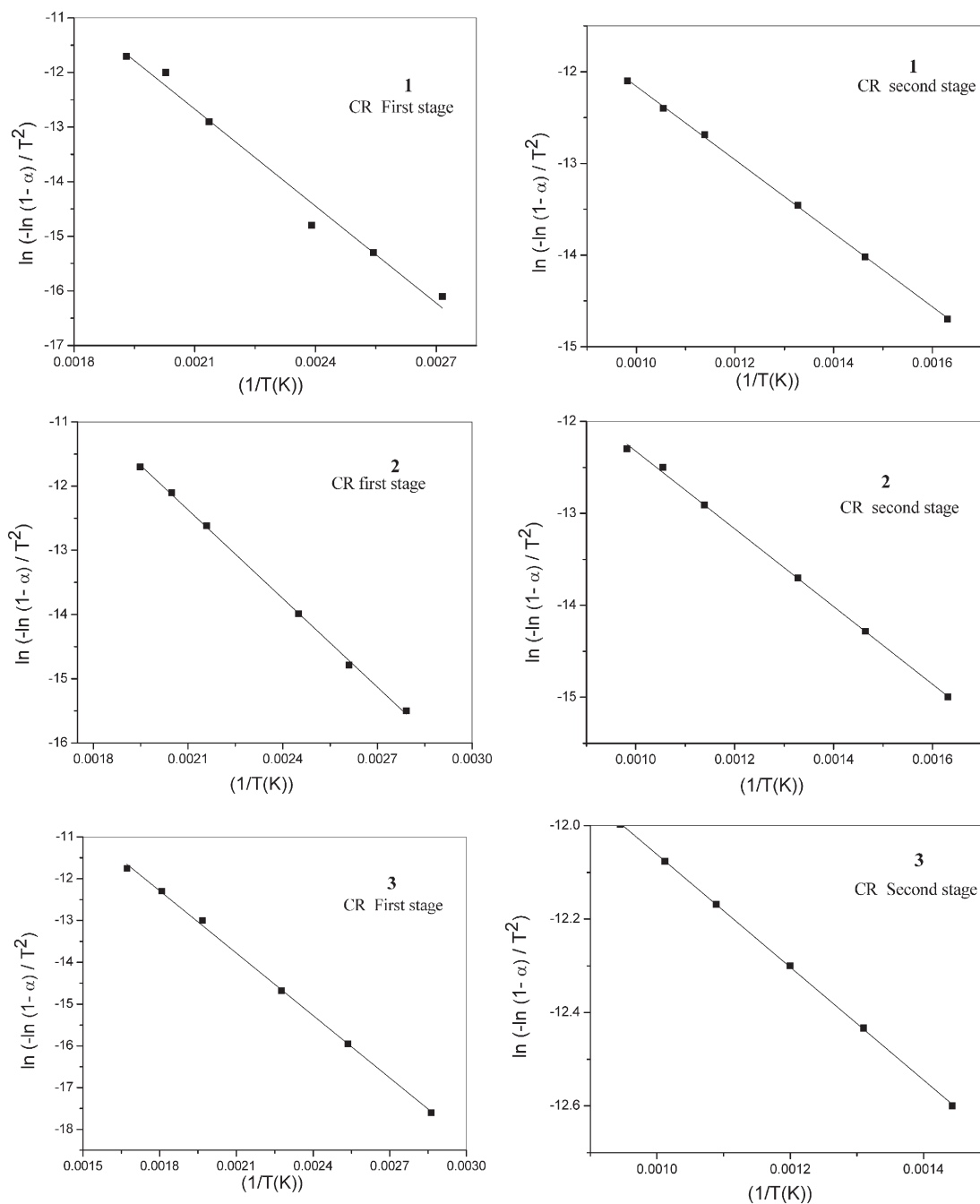


Fig. 17. Coats–Redfern (CR) of Ru(III) complexes (1–3).

where  $k_B$  is the Boltzmann constant,  $h$  is the Plank's constant and  $T_s$  is the TG peak temperature.

### 3.10.2. Horowitz–Metzger equation

The Horowitz–Metzger equation is an illustrative of the approximation methods. These authors derived the relation:

$$\log \left[ \frac{1 - (1 - \alpha)^{1-n}}{1-n} \right] = \frac{E_a \theta}{2.303RT_s^2}, \text{ for } n \neq 1 \quad (14)$$

when  $n = 1$ , the LHS of Eq. (14) would be  $\log[-\log(1 - \alpha)]$  (Figs. 18 and 19). For a first order kinetic process, the Horowitz–Metzger equation

may write in the form:

$$\log \left[ \log \left( \frac{W_\alpha}{W_\gamma} \right) \right] = \frac{E_a \theta}{\log 2.303} \quad (15)$$

where  $\theta = T - T_s$ ,  $w_\gamma = w_\alpha - w$ ,  $w_\alpha$  = mass loss at the completion reaction; and  $w$  = mass loss up to time  $t$ . The plot of  $\log [\log (w_\alpha/w_\gamma)]$  vs.  $\theta$  was drawn and found to be linear from the slope of which  $E_a$  was calculated. The pre-exponential factor,  $A$ , calculated from equation:

$$\frac{E_a}{RT_s^2} = \frac{A}{\left[ \varphi \exp \left( -\frac{E_a}{RT_s} \right) \right]} \quad (16)$$

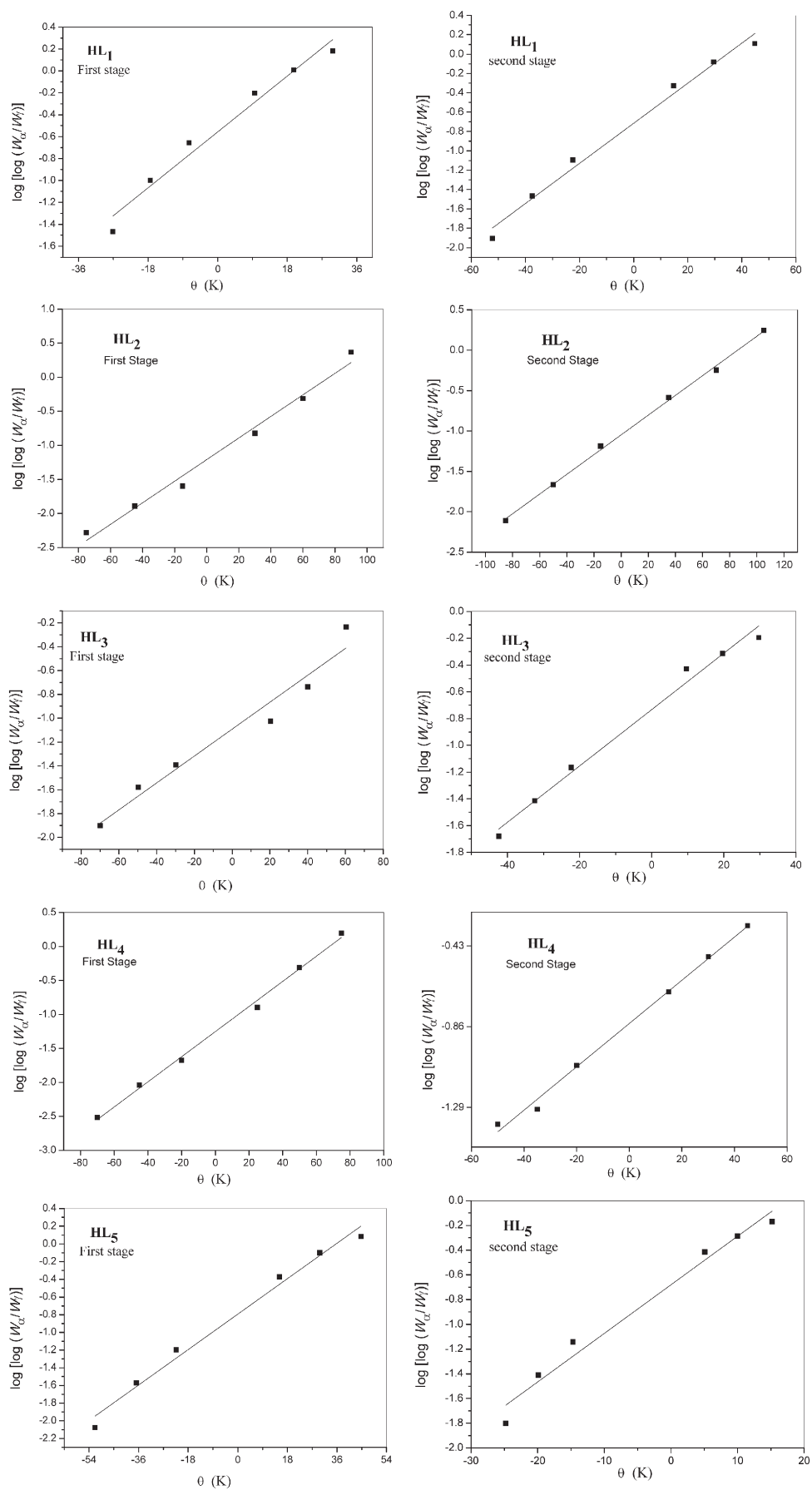


Fig. 18. Horowitz-Metzger (HM) of the ligands (HL<sub>n</sub>).

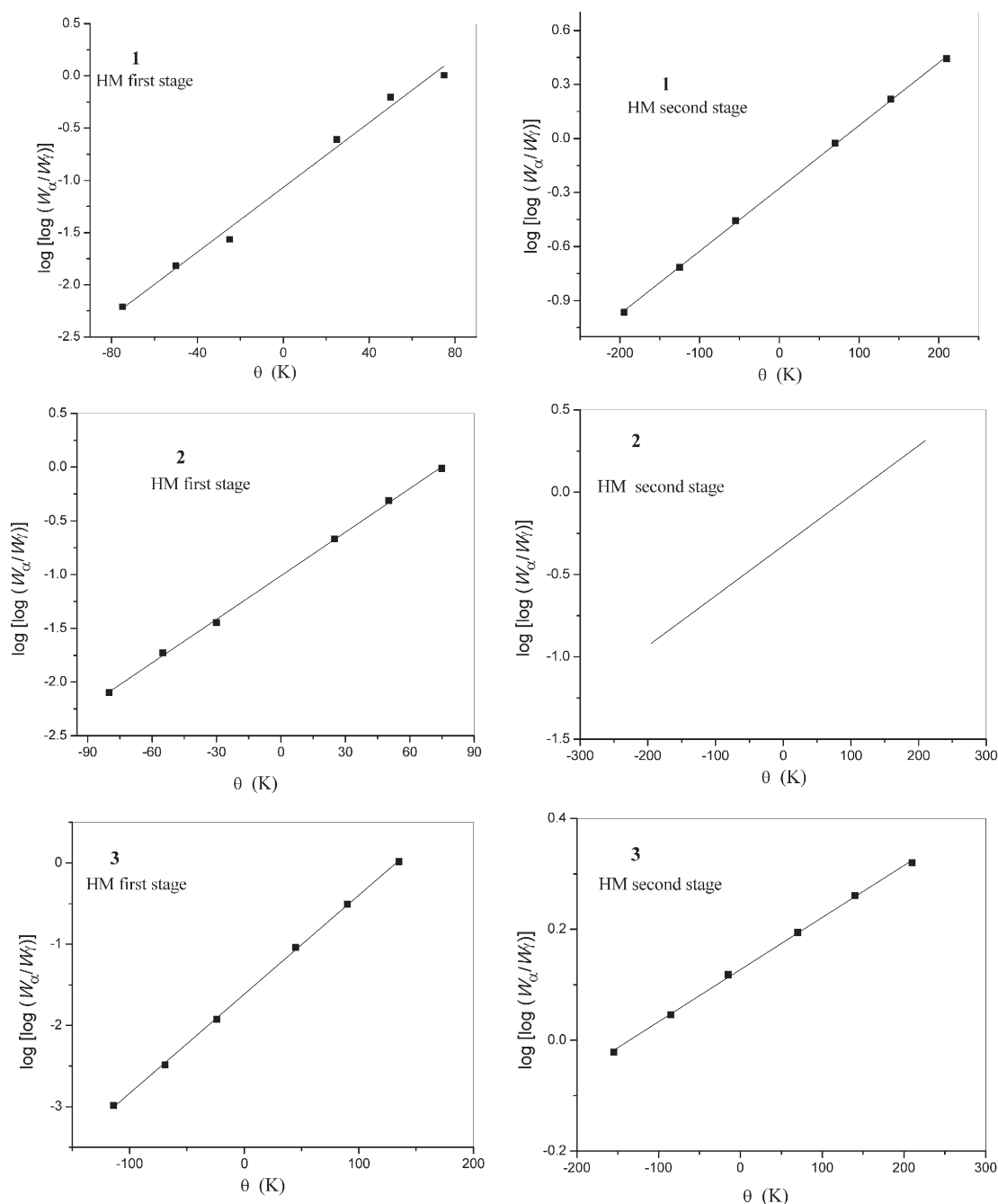


Fig. 19. Horowitz–Metzger (HM) of Ru(III) complexes (1–3).

The entropy of activation,  $\Delta S^*$ , is calculated from Eq. (13). The enthalpy activation,  $\Delta H^*$ , and Gibbs free energy,  $\Delta G^*$ , calculated from:

$$\Delta H^* = E_a - RT \quad (17)$$

$$\Delta G^* = \Delta H^* - T \Delta S^* \quad (18)$$

The calculated values of  $E_a$ ,  $A$ ,  $\Delta S^*$ ,  $\Delta H^*$  and  $\Delta G^*$  for the decomposition steps for ligands ( $HL_n$ ) and Ru(III) complexes (1–3) are summarized in Table 9.

The high values of the activation energies ( $E_a$ ) reflect the thermal stability of the compounds. The ligand  $HL_5$  is the highest value of  $E_a$ . This indicates that, the ligand  $HL_5$  is more thermally stable than the other ligands.

The negative values of activation entropies ( $\Delta S^*$ ) indicate a more ordered activated compounds than the reactants and/or the reactions are slow [22]. The values of  $\Delta G^*$  is positive considered as favorable or spontaneous reaction.

### 3.11. DNA binding studies

Absorption titration is one of the most universally employed methods to study the binding modes and binding extent of compounds to DNA. Absorption titration experiments are performed with fixed concentrations of the ligands ( $HL_1$ ,  $HL_3$  and  $HL_5$ ) and Ru(III) complexes (1–3) (40  $\mu$ M) while gradually increasing the concentration of DNA (10 mM) at 25 °C. While measuring the absorption spectra, an equal amount of DNA was added to both the compound solution and the reference solution to eliminate the absorbance of DNA itself. We have

**Table 9**  
Thermodynamic data of the thermal decomposition of ligands (HL<sub>n</sub>) and Ru(III) complexes (1–3).

Compound <sup>a</sup>	Decomposition temperature (°C)	Method	Parameter					Correlation coefficient (r)
			E <sub>a</sub> (kJ mol <sup>-1</sup> )	A (s <sup>-1</sup> )	ΔS* (J mol <sup>-1</sup> K <sup>-1</sup> )	ΔH* (kJ mol <sup>-1</sup> )	ΔG* (kJ mol <sup>-1</sup> )	
HL <sub>1</sub>	First	CR	68.9	5.29 × 10 <sup>7</sup>	-0.989 × 10 <sup>2</sup>	65.8	102	0.9774
		HM	74.5	5.19 × 10 <sup>8</sup>	-0.799 × 10 <sup>2</sup>	71.4	101	0.9674
	Second	CR	91.1	1.37 × 10 <sup>7</sup>	-1.13 × 10 <sup>2</sup>	86.9	144	0.9942
		HM	101	3.51 × 10 <sup>8</sup>	-0.857 × 10 <sup>2</sup>	97.1	140	0.9858
HL <sub>2</sub>	First	CR	57.9	4.16 × 10 <sup>3</sup>	-1.79 × 10 <sup>2</sup>	54.0	138	0.9978
		HM	66.6	2.44 × 10 <sup>5</sup>	-1.46 × 10 <sup>2</sup>	62.7	131	0.9827
	Second	CR	104	1.14 × 10 <sup>5</sup>	-1.55 × 10 <sup>2</sup>	98.2	206	0.9999
		HM	113	2.19 × 10 <sup>6</sup>	-1.31 × 10 <sup>2</sup>	107	197	0.9980
HL <sub>3</sub>	First	CR	40.4	2.52 × 10 <sup>1</sup>	-2.22 × 10 <sup>2</sup>	36.4	144	0.9044
		HM	50.5	1.86 × 10 <sup>3</sup>	-1.86 × 10 <sup>2</sup>	46.4	136	0.9492
	Second	CR	175	9.85 × 10 <sup>10</sup>	-0.414 × 10 <sup>2</sup>	169	197	0.9899
		HM	189	3.25 × 10 <sup>12</sup>	-0.123 × 10 <sup>2</sup>	184	192	0.9863
HL <sub>4</sub>	First	CR	72.1	7.65 × 10 <sup>4</sup>	-1.55 × 10 <sup>2</sup>	68.1	142	0.9974
		HM	80.9	4.90 × 10 <sup>6</sup>	-1.21 × 10 <sup>2</sup>	77.0	135	0.9951
	Second	CR	77.9	3.08 × 10 <sup>3</sup>	-1.84 × 10 <sup>2</sup>	72.6	190	0.9975
		HM	89.8	9.96 × 10 <sup>4</sup>	-1.56 × 10 <sup>2</sup>	84.5	184	0.9942
HL <sub>5</sub>	First	CR	86.6	1.59 × 10 <sup>7</sup>	-1.11 × 10 <sup>2</sup>	82.7	135	0.9932
		HM	96.3	4.88 × 10 <sup>8</sup>	-0.825 × 10 <sup>2</sup>	92.4	132	0.9840
	Second	CR	301	1.84 × 10 <sup>22</sup>	-1.75 × 10 <sup>2</sup>	295	182	0.9752
		HM	316	6.58 × 10 <sup>23</sup>	-2.05 × 10 <sup>2</sup>	311	178	0.9729
(1)	First	CR	49.2	7.77 × 10 <sup>2</sup>	-1.93 × 10 <sup>2</sup>	45.5	131	0.9801
		HM	58.2	4.36 × 10 <sup>4</sup>	-1.59 × 10 <sup>2</sup>	54.6	125	0.9902
(2)	Second	CR	33.3	1.92 × 10 <sup>-1</sup>	-2.67 × 10 <sup>2</sup>	26.6	242	0.9995
		HM	43.6	8.87 × 10 <sup>-1</sup>	-2.54 × 10 <sup>2</sup>	36.9	242	0.9996
	First	CR	38.2	7.64 × 10 <sup>1</sup>	-2.12 × 10 <sup>2</sup>	34.6	128	0.9989
		HM	49.7	6.55 × 10 <sup>3</sup>	-1.75 × 10 <sup>2</sup>	46.1	123	0.9991
(3)	Second	CR	35.1	3.21 × 10 <sup>-1</sup>	-2.63 × 10 <sup>2</sup>	28.4	241	0.9987
		HM	38.0	5.02 × 10 <sup>-1</sup>	-2.59 × 10 <sup>2</sup>	31.3	241	0.9990
	First	CR	41.4	4.43 × 10 <sup>1</sup>	-2.17 × 10 <sup>2</sup>	37.5	138	0.9986
		HM	50.1	3.11 × 10 <sup>3</sup>	-1.82 × 10 <sup>2</sup>	46.2	130	0.9996
Second	CR	10.0	5.83 × 10 <sup>-3</sup>	-2.96 × 10 <sup>2</sup>	2.99	254	0.9998	
	HM	12.9	3.39 × 10 <sup>-3</sup>	-3.01 × 10 <sup>2</sup>	5.89	261	0.9990	

<sup>a</sup> Numbers as given in Table 1.

determine the intrinsic binding constant to CT-DNA by monitoring the absorption intensity of the charge transfer spectral bands near 393, 388 and 474 nm for the ligands (HL<sub>1</sub>, HL<sub>3</sub> and HL<sub>5</sub>), respectively and 423, 484 and 536 nm for Ru(III) complexes (1–3), respectively. The absorption spectra of these ligands and Ru(III) complexes with increasing concentration of CT-DNA are in the range 300–700 nm.

Upon the addition of increasing amount of CT-DNA, a significant “hypochromic” effect was observed. The obvious hypochromism indicates the non-covalently intercalative binding of compounds to DNA helix, due to the strong stacking interaction between the aromatic chromophores of the compound and base pairs of DNA [52]. The intrinsic binding constants (K<sub>b</sub>) of the ligands (HL<sub>1</sub>, HL<sub>3</sub> and HL<sub>5</sub>) and Ru(III) complexes (1–3) with CT-DNA were determined (Eq. (1)) [16,53].

The K<sub>b</sub> values obtained from the absorption spectral technique for ligands (HL<sub>1</sub>, HL<sub>3</sub> and HL<sub>5</sub>) were calculated as 3.21 × 10<sup>4</sup>, 5.48 × 10<sup>4</sup> and 9.12 × 10<sup>4</sup> M<sup>-1</sup>, respectively. The K<sub>b</sub> values obtained from the absorption spectral technique for Ru(III) complexes (1–3) were calculated as 1.90 × 10<sup>5</sup>, 3.92 × 10<sup>5</sup> and 8.68 × 10<sup>5</sup> M<sup>-1</sup>, respectively. The binding constant of the complexes (1–3) are comparatively higher than that of the ligands (HL<sub>1</sub>, HL<sub>3</sub> and HL<sub>5</sub>). The K<sub>b</sub> values are consistent with Hammett's constant (σ<sup>R</sup>) as shown in Fig. 20. The higher value of the binding constant of HL<sub>5</sub> ligand is due to the presence of electron withdrawing group NO<sub>2</sub>.

### 3.12. Antimicrobial activity

Antibacterial and antifungal activities of ligands (HL<sub>n</sub>) and Ru(III) complexes (1–3) are tested against the Gram positive bacteria (*S. aureus* and *B. cereus*), Gram negative bacteria (*E. coli* and *K. pneumoniae*) and fungal species (*A. niger*, *F. oxysporium*, *P. italicum* and *A. alternata*).

The results of the antibacterial activity of ligands (HL<sub>n</sub>) and Ru(III) complexes (1–3) are listed in Table 10. The ligands (HL<sub>n</sub>) and Ru(III) complexes (1–3) have no antibacterial activity except complexes (1) and (2) showed good antibacterial activity against *B. cereus* as shown in Fig. S1 in the supplementary. It was found that the complex (1) was more potent antibacterial activity 10, 12 and 12 mm at concentrations 50, 100 and 150 µg/ml, respectively, than the other complexes against *B. cereus* (Table 10).

The results of the antifungal activity of ligands (HL<sub>n</sub>) and Ru(III) complexes were listed in Table 11. It was found that the ligands and Ru(III) complexes have no antifungal activity against *F. oxysporum* and *P. italicum*. The compounds HL<sub>2</sub> and HL<sub>3</sub> showed antifungal activity against *A. niger* at high concentration 3, 3 and 7 mm at concentrations 150, 100 and 150 µg/ml, respectively, as shown in Fig. S2 in the supplementary. The ligand HL<sub>5</sub> showed antifungal activity against *A. niger* and *A. alternata* (4 and 2 mm) at all the prepared concentrations [8,11].

### 3.13. Catalytic oxidation of cyclohexanol to cyclohexanone

Ruthenium mediated oxidations are finding increasing application due to the unique properties of this extremely versatile transition metal, whose oxidation states can vary from -2 to +8 and this prompted us to carry out this type of reaction. The present work describes the catalytic oxidation of secondary alcohol by the synthesized ruthenium (III) complexes in CH<sub>2</sub>Cl<sub>2</sub> in the presence of periodic acid (Scheme 3).

No oxidation of cyclohexanol to cyclohexanone was achieved employing IO(OH)<sub>5</sub> only. Thus, the catalytic oxidation of cyclohexanol to cyclohexanone by the precursor catalysts [Ru(L<sub>n</sub>)(AsPh<sub>3</sub>)<sub>2</sub>Cl<sub>2</sub>]<sub>x</sub>H<sub>2</sub>O (n = 1, 3 and 5) under ultrasonic irradiation and in the presence of IO(OH)<sub>5</sub> (1:200 M ratio of catalyst to substrate) at room temperature in CH<sub>2</sub>Cl<sub>2</sub>/CH<sub>3</sub>CN mixture was carried out. The formed ketone was

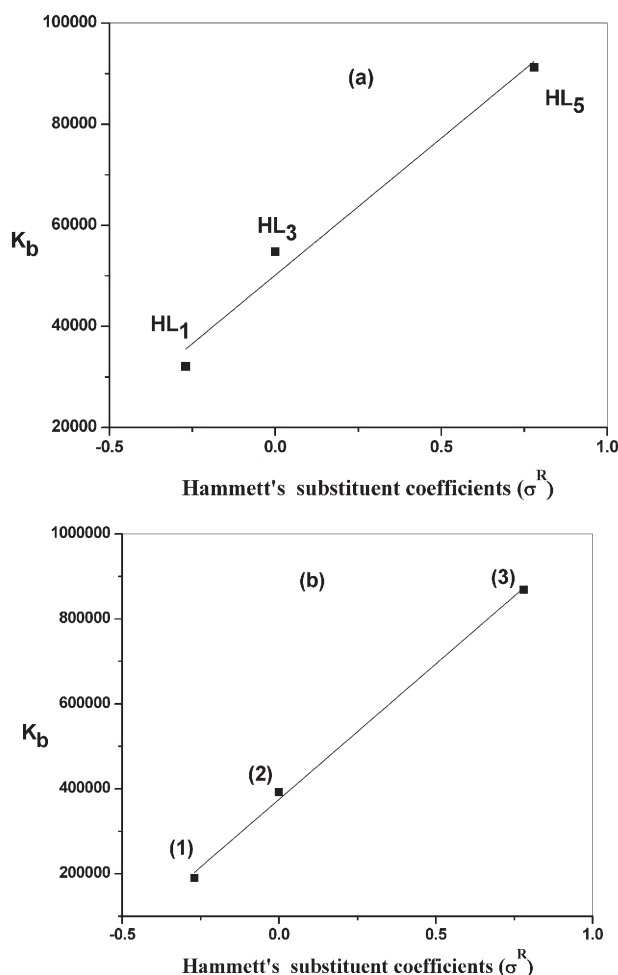


**Fig. 20.** The relation between Hammett's substitution coefficient ( $\sigma^R$ ) vs.  $K_b$  for (a) ligands (HL<sub>1</sub>, HL<sub>3</sub> and HL<sub>5</sub>) and (b) complexes (1–3).

quantified as its 2,4-dinitrophenylhydrazone derivatives. There was no detectable oxidation in the absence of ruthenium complexes. The catalytic oxidation of different substrates as benzyl alcohol, 2-butanol, 1-phenylethanol, cyclopentanol, styryl carbinol and cyclohexanol using ruthenium complexes as catalyst were reported [54,55].

Experimental yield was 65, 48 and 83% with TOF 9, 7 and 12 for 1, 2 and 3, respectively. The mechanism of oxidation of cyclohexanol to cyclohexanone by the catalysts  $[\text{Ru}(\text{L}_n)(\text{AsPh}_3)_2\text{Cl}_2] \cdot x\text{H}_2\text{O}$  ( $n = 1, 3$  and 5) in the presence of the co-oxidant could be proceeded via the formation of oxoruthenium (IV) intermediate species which are capable to abstract hydrogen atom from the OH group in cyclohexanol [56].

#### 4. Conclusion

Ruthenium (III) complexes of 5-(4-derivative phenyl azo)-8-hydroxyquinoline ligands (HL<sub>n</sub>) have been synthesized and structurally characterized. Octahedral complexes of the general formula  $[\text{Ru}(\text{L}_n)(\text{AsPh}_3)_2\text{Cl}_2] \cdot x\text{H}_2\text{O}$  ( $\text{L} =$  the anions of the ligands (HL<sub>n</sub>)) are proposed. The optimized bond lengths, bond angles and calculated the quantum chemical parameters for the ligands (HL<sub>n</sub>) and Ru(III) complexes are investigated. The thermogravimetric analysis of the complexes shows metal oxide remaining as the final product. The values of activation energies of decomposition ( $E_a$ ) for ligands and Ru(III) complexes are calculated. It was found that the values of  $E_a$  depending on the nature of substituent. It was found that the complex (3) is more stable than the other complexes. The higher value of the binding constant of HL<sub>5</sub> ligand is due to the presence of electron

**Table 10**

Antibacterial activity data of the ligands (HL<sub>n</sub>) and Ru(III) complexes (1–3). The results are recorded as the diameter of inhibition zone (mm).

Compound <sup>a</sup>	Conc. (μg/ml)	Gram positive bacteria		Gram negative bacteria	
		<i>Bacillus cereus</i>	<i>Staphylococcus aureus</i>	<i>Escherichia coli</i>	<i>Klebsiella pneumoniae</i>
HL <sub>1</sub>	50	–ve	–ve	–ve	–ve
	100	–ve	–ve	–ve	–ve
	150	–ve	–ve	–ve	–ve
HL <sub>2</sub>	50	–ve	–ve	–ve	–ve
	100	–ve	–ve	–ve	–ve
	150	–ve	–ve	–ve	–ve
HL <sub>3</sub>	50	–ve	–ve	–ve	–ve
	100	–ve	–ve	–ve	–ve
	150	–ve	–ve	–ve	–ve
HL <sub>4</sub>	50	–ve	–ve	–ve	–ve
	100	–ve	–ve	–ve	–ve
	150	–ve	–ve	–ve	–ve
HL <sub>5</sub>	50	–ve	–ve	–ve	–ve
	100	–ve	–ve	–ve	–ve
	150	–ve	–ve	–ve	–ve
(1)	50	10	–ve	–ve	–ve
	100	12	–ve	–ve	–ve
	150	12	–ve	–ve	–ve
(2)	50	10	–ve	–ve	–ve
	100	10	–ve	–ve	–ve
	150	10	–ve	–ve	–ve
(3)	50	–ve	–ve	–ve	–ve
	100	–ve	–ve	–ve	–ve
	150	–ve	–ve	–ve	–ve
Penicillin	50	1	2	1	–ve
	100	3	2	3	–ve
	150	3	2	3	–ve

<sup>a</sup> Numbers as given in Table 1.

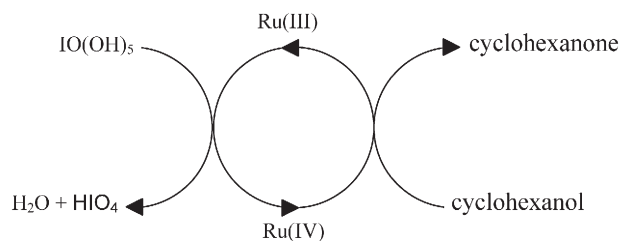
withdrawing group NO<sub>2</sub>. Complexes (1) and (2) have good antibacterial activity against *B. cereus* and HL<sub>2</sub>, HL<sub>3</sub> and HL<sub>5</sub> ligands have good antifungal activity against *A. niger* and also HL<sub>5</sub> showed against *A. alternata*. The Ru(III) complexes were found to be effective catalyst

**Table 11**

Antifungal activity data of the ligands (HL<sub>n</sub>) and Ru(III) complexes (1–3). The results were recorded as the diameter of inhibition zone (mm).

Compound <sup>a</sup>	Conc. (μg/ml)	<i>Aspergillus niger</i>	<i>Fusarium oxysporum</i>	<i>Alternaria alternata</i>	<i>Penicillium italicum</i>
HL <sub>1</sub>	50	–ve	–ve	–ve	–ve
	100	–ve	–ve	–ve	–ve
	150	–ve	–ve	–ve	–ve
HL <sub>2</sub>	50	–ve	–ve	–ve	–ve
	100	2	–ve	–ve	–ve
	150	3	–ve	–ve	–ve
HL <sub>3</sub>	50	2	–ve	–ve	–ve
	100	3	–ve	–ve	–ve
	150	7	–ve	–ve	–ve
HL <sub>4</sub>	50	–ve	–ve	–ve	–ve
	100	–ve	–ve	–ve	–ve
	150	–ve	–ve	–ve	–ve
HL <sub>5</sub>	50	4	–ve	2	–ve
	100	4	–ve	2	–ve
	150	4	–ve	2	–ve
(1)	50	–ve	–ve	–ve	–ve
	100	–ve	–ve	–ve	–ve
	150	–ve	–ve	–ve	–ve
(2)	50	–ve	–ve	–ve	–ve
	100	–ve	–ve	–ve	–ve
	150	–ve	–ve	3	–ve
(3)	50	–ve	–ve	–ve	–ve
	100	–ve	–ve	–ve	–ve
	150	–ve	–ve	–ve	–ve
Miconazole	50	1	2	5	1
	100	3	3	6	1
	150	4	3	6	2

<sup>a</sup> Numbers as given in Table 1.



**Scheme 3.** Catalytic cycle for the catalytic oxidation of cyclohexanol to cyclohexanone by  $[\text{Ru}(\text{L}_n)(\text{AsPh}_3)_2\text{Cl}_2]/\text{IO}(\text{OH})_5$ .

for the oxidation of cyclohexanol to cyclohexanone in the presence of  $\text{IO}(\text{OH})_5$  as co-oxidant.

### Acknowledgement

The authors would like to thank Prof. Dr. M.I. Abou-Dobara and Miss. N.F. Omar, Botany Department, Faculty of Science, Damietta University, Egypt for their help during testing antimicrobial activity.

### Appendix A. Supplementary data

Supplementary data to this article can be found online at <http://dx.doi.org/10.1016/j.molliq.2016.02.043>.

### References

- [1] N.A. El-Ghamaz, E.M. El-Menyawy, M.A. Diab, A.A. El-Bindary, A.Z. El-Sonbati, S.G. Nozha, *Solid State Sci.* 30 (2014) 44–54.
- [2] N.A. El-Ghamaz, M.A. Diab, A.A. El-Bindary, A.Z. El-Sonbati, S.G. Nozha, *Spectrochim. Acta A* 143 (2015) 200–212.
- [3] M.A. Diab, A.Z. El-Sonbati, A.A. El-Bindary, A.M. Barakat, *Spectrochim. Acta A* 116 (2013) 428–439.
- [4] M.A. Diab, A.A. El-Bindary, A.Z. El-Sonbati, O.L. Salem, *J. Mol. Struct.* 1018 (2012) 176–184.
- [5] M. Albrecht, O. Blau, R. Frohlich, *Chem. Eur. J.* 5 (1999) 48–56.
- [6] M.A. Diab, A.A. El-Bindary, A.Z. El-Sonbati, O.L. Salem, *J. Mol. Struct.* 1007 (2012) 11–19.
- [7] N.A. El-Ghamaz, M.A. Diab, A.Z. El-Sonbati, O.L. Salem, *Spectrochim. Acta A* 83 (2011) 61–66.
- [8] M.I. Abou-Dobara, A.Z. El-Sonbati, Sh.M. Morgan, *World J. Microbiol. Biotechnol.* 29 (2013) 119–126.
- [9] A.U. Patel, *E-J. Chem.* 6 (2009) 1247–1252.
- [10] M.A. Diab, A.Z. El-Sonbati, A.A. El-Bindary, G.G. Mohamed, Sh.M. Morgan, *Res. Chem. Intermed.* 41 (2015) 9029–9066.
- [11] A.S.A. Zidan, *J. Therm. Anal. Calorim.* 68 (2002) 1045–1059.
- [12] A.Z. El-Sonbati, M.A. Diab, A.A. El-Bindary, G.G. Mohamed, Sh.M. Morgan, M.I. Abou-Dobara, S.G. Nozha, *J. Mol. Liq.* 215 (2016) 423–442.
- [13] A.K.A. Hadi, *Pol. J. Chem.* 68 (1994) 803–806.
- [14] A.Z. El-Sonbati, M.A. Diab, *Physico-chemical Studies on the Complexes, LAMBERT Academic Publishing GmbH, Leipzig & Co. KG, Germany, 2010 (ISBN: 978-3-8433-7229-9)*.
- [15] A.Z. El-Sonbati, M.A. Diab, A.A. El-Bindary, *Stoichiometry and Research—The Importance of Quantity in Biomedicine*, Pub. by In Tech, Janeza Trdine 9, 51000 Rijeka, Croatia, 2012 147–194 P. Cm, ISBN 978-953-51-0198-7.
- [16] A.F. Shoair, A.R. El-Shobaky, E.A. Azab, *Spectrochim. Acta A* 151 (2015) 322–334.
- [17] N.A. El-Ghamaz, A.A. El-Bindary, A.Z. El-Sonbati, N.M. Beshry, *J. Mol. Liq.* 211 (2015) 628–639.
- [18] A.Z. El-Sonbati, A.A. El-Bindary, A.F. Shoair, R.M. Younes, *Chem. Pharm. Bull.* 49 (2001) 1308–1313.
- [19] M.J. Waring, *J. Mol. Biol.* 13 (1965) 269–282.
- [20] A.Z. El-Sonbati, A.F. Shoair, A.A. El-Bindary, A.S. Mohamed, *J. Mol. Liq.* 209 (2015) 635–647.
- [21] A. Wolfe, G.H. Shimer, T. Meehan, *Biochemistry* 26 (1987) 6392–6396.
- [22] N.A. El-Ghamaz, A.Z. El-Sonbati, M.A. Diab, A.A. El-Bindary, G.G. Mohamed, Sh.M. Morgan, *Inorg. Chim. Acta* 430 (2015) 96–107.
- [23] A.F. Shoair, *J. Coord. Chem.* 65 (2012) 3511–3518.
- [24] N.A. El-Ghamaz, A.Z. El-Sonbati, M.A. Diab, A.A. El-Bindary, G.G. Mohamed, Sh.M. Morgan, *Spectrochim. Acta A* 147 (2015) 200–211.
- [25] A.Z. El-Sonbati, M.A. Diab, A.A. El-Bindary, A.M. Eldesoky, Sh.M. Morgan, *Spectrochim. Acta A* 135 (2015) 774–791.
- [26] A.Z. El-Sonbati, G.G. Mohamed, A.A. El-Bindary, W.M.I. Hassan, A.K. Elkholy, *J. Mol. Liq.* 209 (2015) 625–634.
- [27] A.Z. El-Sonbati, G.G. Mohamed, A.A. El-Bindary, W.M.I. Hassan, M.A. Diab, Sh.M. Morgan, A.K. Elkholy, *J. Mol. Liq.* 212 (2015) 487–502.
- [28] A. Halgren, *J. Computat. Chem.* 17 (1998) 490–519.
- [29] G.M. Morris, D.S. Goodsell, *J. Comput. Chem.* 19 (1998) 1639–1662.
- [30] G. Cook, V.M. Rotello, *Chem. Soc. Rev.* 31 (2002) 275–286.
- [31] M. Albrecht, K. Witt, E. Wegelins, K. Rissanen, *Tetrahedron* 56 (2000) 591–594.
- [32] M. Albrecht, O. Blau, E. Wegelins, K. Rissanen, *New J. Chem.* 23 (1999) 667–668.
- [33] N.A. El-Ghamaz, A.Z. El-Sonbati, M.A. Diab, A.A. El-Bindary, M.K. Awad, Sh.M. Morgan, *Mater. Sci. Semicond. Process.* 19 (2014) 150–162.
- [34] A.A. El-Bindary, A.Z. El-Sonbati, M.A. Diab, Sh.M. Morgan, *J. Mol. Liq.* 201 (2015) 36–42.
- [35] N.A. El-Ghamaz, M.A. Diab, A.A. El-Bindary, A.Z. El-Sonbati, H.A. Seyam, *Mater. Sci. Semicond. Process.* 27 (2014) 521–531.
- [36] C. Hammond, *The Basics of Crystallography and Diffraction*, third ed. Oxford University Press, 2009.
- [37] A.Z. El-Sonbati, R.M. Issa, A.M. Abd El-Gawad, *Spectrochim. Acta A* 68 (2007) 134–138.
- [38] M. Albrecht, K. Witte, R. Frohlich, O. Kataeva, *Tetrahedron* 58 (2002) 561–567.
- [39] A.Z. El-Sonbati, A.A. El-Bindary, *Pol. J. Chem.* 74 (2000) 621–630.
- [40] E. Bardez, I. Devol, B. Larry, B. Valeur, *J. Phys. Chem. B* 101 (1997) 7786–7793.
- [41] M. Albrecht, O. Blau, E. Wegelins, K. Rissanen, *New J. Chem.* 23 (1999) 667–668.
- [42] G. Cook, V.M. Rotello, *Chem. Soc. Rev.* 31 (2002) 275–286.
- [43] A. Teimouri, A.N. Chemmahini, K. Taban, H.A. Dabbagh, *Spectrochim. Acta A* 72 (2009) 369–377.
- [44] V. Krishnakumar, R. Ramasamy, *Spectrochim. Acta A* 61 (2005) 673–683.
- [45] A.Z. El-Sonbati, A.A.M. Belal, S.A. Abd El-Meksoud, R.A. El-Boz, *J. Mol. Struct.* 1027 (2012) 200–206.
- [46] A.Z. El-Sonbati, A.A. Belal, S.I. El-Wakel, M.A. Hussien, *Spectrochim. Acta A* 60 (2004) 965–972.
- [47] W.H. Mahmoud, N.F. Mahmoud, G.G. Mohamed, A.Z. El-Sonbati, A.A. El-Bindary, *J. Mol. Liq.* 1095 (2015) 15–25.
- [48] M.M. Ghoneim, A.Z. El-Sonbati, A.A. El-Bindary, M.A. Diab, L.S. Serag, *Spectrochim. Acta A* 140 (2015) 111–131.
- [49] N.A. El-Ghamaz, A.Z. El-Sonbati, M.A. Diab, A.A. El-Bindary, Sh.M. Morgan, *Mater. Res. Bull.* 65 (2015) 293–301.
- [50] A.W. Coats, J.P. Redfern, *Nature* 20 (1964) 68–79.
- [51] H.W. Horowitz, G. Metzger, *Anal. Chem.* 35 (1963) 1464–1468.
- [52] Y. Liu, K. Zhang, Y. Wu, J. Zhao, J. Liu, *Chem. Biodivers.* 9 (2012) 1533–1544.
- [53] J.P. Costes, F. Dahan, J.P. Laurent, M. Drillon, *Inorg. Chem. Acta* 294 (1999) 8–13.
- [54] M. Brissard, O. Convert, M. Gruselle, C. Guyard-Duhayon, R. Thouvenot, *Inorg. Chem.* 42 (2003) 1378–1385.
- [55] H. Masui, A.B.P. Lever, P.R. Auburn, *Inorg. Chem.* 30 (1991) 2402–2410.
- [56] J.T. Warren, W. Chen, D.H. Johnston, C. Turro, *Inorg. Chem.* 38 (1999) 6187–6192.